

# Dynamic stability of complex networks

Chandrakala Meena<sup>1,2</sup>, Chittaranjan Hens<sup>3</sup>, Simcha Haber<sup>1</sup>, Stefano Boccaletti<sup>4-6</sup>  
& Baruch Barzel<sup>1,2,\*</sup>

1. Department of Mathematics, Bar-Ilan University, Ramat-Gan, Israel
  2. Gonda Multidisciplinary Brain Research Center, Bar-Ilan University, Ramat-Gan, Israel
  3. Physics and Applied Mathematics Unit, Indian Statistical Institute, Kolkata, India
  4. CNR - Institute of Complex Systems, Via Madonna del Piano 10, Sesto Fiorentino I-50019, Italy
  5. Unmanned Systems Research Institute, Northwestern Polytechnical University, Xi'an 710072, China
  6. Moscow Institute of Physics and Technology (National Research University), 9 Institutskiy per., Dolgoprudny, Moscow Region 141701, Russian Federation
- \* **Correspondence:** baruchbarzel@gmail.com

*In memory of Prof. Robert May*

**Will a large complex system be stable? This question, first posed by May in 1972, captures a long standing challenge, fueled by a seeming contradiction between theory and practice. While empirical reality answers with an astounding yes, the mathematical analysis, based on linear stability theory, seems to suggest the contrary - hence, the diversity-stability paradox. Here we present a solution to this dichotomy, by considering the interplay between topology and dynamics. We show that this interplay leads to the emergence of non-random patterns in the system's stability matrix, leading us to relinquish the prevailing random matrix-based paradigm. Instead, we offer a new matrix ensemble, which captures the dynamic stability of real-world systems. This ensemble helps us analytically identify the relevant control parameters that predict a system's stability, exposing three broad dynamic classes: In the asymptotically unstable class, diversity, indeed, leads to instability *à la* May's paradox. However, we also expose an asymptotically stable class, the class in which most real systems reside, in which diversity not only does not prohibit, but, in fact, enhances dynamic stability. Finally, in the sensitively stable class diversity plays no role, and hence stability is driven by the system's microscopic parameters. Together, our theory uncovers the naturally emerging rules of complex system stability, helping us reconcile the paradox that has eluded us for decades.**

The study of complex social, biological and technological systems, is often directed towards dramatic events, such as cascading failures<sup>1-5</sup> or abrupt state transitions<sup>3,6,8,9</sup>. In reality, however, these represent the exception rather than the rule. In fact, the truly intriguing mathematical puzzle is how, despite enduring constant perturbations and local obstructions, these systems continue to sustain reliably stable functionality<sup>10-13</sup>. This challenge is rooted in the *diversity-stability paradox*<sup>6</sup>, which predicts that a sufficiently large complex system, will inevitably become unstable. What, then, are the naturally emerging organizing principles, or in May's original wording - *what are nature's devious strategies*, to achieve this ubiquitously observed dynamic stability?

Initial clues began to unveil with the mapping of empirical networks, which uncovered universally recurring topological characteristics<sup>4,16,17</sup> that can potentially impact the system's dynamics<sup>18</sup>.

For example, degree heterogeneity<sup>15</sup>, community structure<sup>2</sup> and topological symmetries<sup>21</sup> - all naturally emerging features of real-world networks - indeed, impact the system's dynamics. However, on their own, these topological features cannot ensure stability<sup>22</sup>, thus leaving May's mathematical challenge unresolved.

Here, we show that the desired *devious strategies* arise not just from the network *topology*, but mainly from its interplay with the system's intrinsic, often nonlinear, interaction *dynamics*. Constrained by the physical mechanisms that drive the system's interacting components, these dynamics provide the desired, naturally emerging, *design* principles that determine the system's stability. Our analysis shows that, under real-world dynamics, stability can be fully predicted from a small set of relevant parameters that capture the combined contribution of both topology *and* dynamics. Most crucially, we identify a broad class of frequently encountered mechanisms, for which a large complex system can, and, at times, even *must* be stable, therefore settling the long overdue diversity-stability debate<sup>23</sup>.

## The diversity-stability challenge

Consider a complex system of  $N$  interacting components (nodes), whose dynamic activities  $\mathbf{x}(t) = (x_1(t), \dots, x_N(t))$  are driven by nonlinear pairwise interactions. The system's fixed-points capture static states, which, unperturbed, remain independent of time. The stability of these fixed-point can be examined through their response to small perturbations  $\delta\mathbf{x}$ , which, in the linear regime, can be approximated by

$$\frac{d\delta\mathbf{x}}{dt} = J\delta\mathbf{x} + O(\delta\mathbf{x}^2), \quad (1)$$

where  $J$  represents the system's Jacobian matrix. We express  $J$  as<sup>6</sup>

$$J = W - CI, \quad (2)$$

in which the off-diagonal elements  $W_{ij}$ , extracted from an arbitrary distribution  $P(w)$ , capture the direct (linear) impact of node  $j$  on node  $i$  (often  $P(w)$  is taken to be a normal distribution  $\mathcal{N}(0, \sigma^2)$ ). Using  $I$  to represent the identity matrix,  $J$ 's diagonal terms  $J_{ii} = -C$ , capture the typical relaxation times of all the nodes, which are dictated by the system's specific rate parameters. Together,  $P(w)$  and  $C$  define the random *matrix ensemble* from which  $J$  is extracted, which we denote by  $\mathbb{E}(P(w), C)$ .

The system  $\mathbb{E}(P(w), C)$  is dynamically stable if  $J$ 's principle eigenvalue satisfies  $\text{Re}(\lambda) < 0$ . The challenge is that, according to random matrix theory, in the limit of large  $N$  we have<sup>6</sup>

$$\text{Re}(\lambda) \sim \sqrt{N} \left( 1 - \frac{C}{\sqrt{N}} \right), \quad (3)$$

which is positive, and hence unstable, as long as  $C < \sqrt{N}$ . Consequently, a sufficiently large system ( $N \rightarrow \infty$ ) becomes inevitably unstable, *i.e.* May's paradox.

**The role of the network topology.** A natural attempt to reconcile this paradox is by considering structural patterns in the interaction network  $A_{ij}$ , which is typically sparse and, most often, highly heterogeneous<sup>4</sup>. As  $J$  is designed to capture the *direct* response between  $i$  and  $j$ , its terms  $J_{ij}$  vanish in case there is no direct  $i, j$  link. We, therefore, write the Jacobian in (2) as  $J = A \otimes W - CI$ , where the Hadamard product  $\otimes$  represents matrix multiplication element

by element. Hence  $J_{ij} = 0$  in case there is no link between  $i$  and  $j$ , and is assigned a weight from  $P(w)$  if  $i$  and  $j$  interact. This provides the Jacobian ensemble  $\mathbb{E}(A_{ij}, P(w), C)$ , in which one first selects the topology  $A_{ij}$ , then assign off-diagonal and diagonal weights from  $P(w)$  and  $C$  (Fig. 1a,b).

In the  $\mathbb{E}(A_{ij}, P(w), C)$  ensemble, the principal eigenvalue  $\lambda$  depends on  $A_{ij}$ 's degree distribution  $P(k)$  through  $\kappa_{\text{nn}} = \langle k^2 \rangle / \langle k \rangle$ , capturing the average nearest neighbor degree<sup>3,22</sup>. The broader is  $P(k)$  the greater is  $\kappa_{\text{nn}}$ , thanks to the second moment  $\langle k^2 \rangle$  that increases with  $P(k)$ 's variance. When sufficiently broad, *i.e.* a fat-tailed  $P(k)$ , we have<sup>2</sup>

$$\kappa_{\text{nn}} \sim N^\beta, \quad (4)$$

an asymptotic divergence with system size. For example, for a scale-free network, in which  $P(k) \sim k^{-\gamma}$  with  $2 < \gamma < 3$ , we have  $\beta = 3 - \gamma$ . Using (3.2) we show that under the  $\mathbb{E}(A_{ij}, P(w), C)$  ensemble the principal eigenvalue follows (Fig. 1c)

$$\text{Re}(\lambda) \sim N^{\frac{\beta}{2}} \left( 1 - \frac{C}{N^{\frac{\beta}{2}}} \right), \quad (5)$$

in which the square-root of (3) is replaced by the exponent  $\beta/2$ . The crucial point is that, once again, we observe an asymptotic behavior that prohibits stability in the limit  $N \rightarrow \infty$ .

*These mathematical observations, now nearing their 50th anniversary, seem to suggest that complex networked systems must be limited in size in order to maintain stability. Reality, however, consistently confronts us with the contrary<sup>23</sup>. To reconcile this incongruity, we next show that under real nonlinear dynamics the structure of  $J$  is fundamentally different from the currently considered Jacobian ensembles. This allows us to fully predict a complex system's dynamic stability, and, down the line, disentangle May's theoretical gridlock.*

## The role of dynamics

The common thread that binds all present treatments of the diversity stability paradox - indeed the *paradigm* - is that one can separate the role of the topology from that of the dynamics. For example, to construct  $J$  in the  $\mathbb{E}(A_{ij}, P(w), C)$  ensemble, one first selects the *topology*  $A_{ij}$ , and then independently extracts the *dynamic* response terms,  $W_{ij}$ , from  $P(w)$ , and the relaxation rate  $C$ . Such construction overlooks the complex interplay between  $A_{ij}$  and  $P(w), C$ , rooted in the nonlinear mechanisms driving the interactions between the nodes. Omitting this interplay is tantamount to ignoring the role of the system's actual nonlinear dynamics. Indeed, in  $\mathbb{E}(P(w), C)$  and  $\mathbb{E}(A_{ij}, P(w), C)$ , if two networks share a similar topology, they will have an equally similar  $J$  (up to statistical variations), regardless of their interaction dynamics - social, biological or technological. This, of course, stands in sharp contrast with the frequently observed fact that different nonlinear mechanisms, despite being run on similar networks, may express fundamentally distinct dynamic behaviors<sup>1,25,26</sup>.

Hence, to truly predict dynamic stability, we derive the mathematical link between  $A_{ij}$  and  $P(w), C$ , seeking the relevant ensemble from which to extract real-world Jacobian matrices.

**Dynamic mechanisms** (Fig. 1d). To construct realistic  $J$  matrices we must consider each system's intrinsic dynamic mechanisms. These mechanisms are inherent to the nature of the system's interacting components: in social systems, for example, individuals interact through

infection and recovery<sup>27–29</sup>, in biological networks, proteins, genes and metabolites are linked through biochemical processes<sup>8,9,31,33</sup>, and in ecological systems, species undergo competitive or symbiotic interactions<sup>11,35,36</sup>. All these processes capture built-in dynamics, representing the *physical* mechanisms that drive all nodes/links. Most generally, these dynamic mechanisms can be described by<sup>1</sup>

$$\frac{dx_i}{dt} = M_0(x_i(t)) + \sum_{j=1}^N A_{ij} M_1(x_i(t)) M_2(x_j(t)), \quad (6)$$

where  $M_0(x)$  captures the self-dynamics of all nodes, and  $M_1(x), M_2(x)$  describe their pairwise interactions. With the appropriate selection of these nonlinear functions Eq. (1.1) captures a broad range of frequently used models in social<sup>27,28</sup>, biological<sup>8,9,11,31,33</sup> and technological<sup>37</sup> systems (Fig. 1g).

**The dynamic Jacobian ensemble** (Fig. 1e). Extracting  $J$  from (1.1), we show in Supplementary Section 1, leads to a currently unexplored matrix ensemble, in which the weights  $J_{ij}$  are strongly intertwined with the topology  $A_{ij}$ , via

$$J_{ii} \sim -C \kappa_{nn}^\eta k_i^\mu \quad (7)$$

$$J_{ij} \sim A_{ij} k_i^\nu k_j^\rho. \quad (8)$$

In (7) and (1.4),  $\kappa_{nn}$  and  $k_i, k_j$  are extracted from the *topology*  $A_{ij}$  and its degree distribution  $P(k)$ . The four exponents,  $\Omega = (\eta, \mu, \nu, \rho)$  are, on the other hand, fully determined by the *dynamics*,  $M_0(x), M_1(x), M_2(x)$ , as shown in **Box I**. The coefficient  $C$ , similar to the Jacobian in (2), represents the system specific rate parameters and characteristic time-scales, a parameter that can potentially be affected by external perturbation or changing environmental conditions<sup>3</sup>.

The result is a non-random Jacobian structure, whose entries, as opposed to the existing ensembles, cannot be selected independently from an arbitrary  $P(w)$ , or set to a constant value  $C$ . Instead (7) and (1.4) define a new ensemble  $\mathbb{E}(A_{ij}, \Omega)$ , which matches, for each underlying network  $A_{ij}$ , a predictable set of weights  $J_{ii}$  and  $J_{ij}$  based on the dynamic exponents  $\Omega$ . Therefore, in contrast to the random matrix based treatment of  $\mathbb{E}(P(w), C)$  or  $\mathbb{E}(A_{ij}, P(w), C)$ , that has led the discussion since May’s original analysis<sup>6</sup>, the newly introduced  $\mathbb{E}(A_{ij}, \Omega)$  captures the effect of the system-specific nonlinear dynamics. Indeed, in (7) and (1.4), identical networks may yield highly distinctive Jacobian matrices, depending on whether the interactions are, *e.g.*, social, biological or ecological, as each dynamics is characterized by its unique set of exponents  $\Omega$ .

To examine this prediction we implemented the dynamics of Fig. 1g on a set of model and relevant empirical networks. This includes four dynamic models: *Social*. The susceptible-infected-susceptible (SIS) model<sup>27,28</sup> for disease spreading; *Regulatory*. The Michaelis-Menten model<sup>8</sup> for gene regulation; *Ecological*. Mutualistic interactions<sup>11</sup> in ecology; *Biochemical*. Protein-protein interactions<sup>9,31,33</sup> in sub-cellular networks. Applying each model to five different networks, we arrive at a total of 20 combinations of networks/dynamics as a testing ground for our predicted  $J$ -ensemble (for a detailed description of all dynamic models and networks see Supplementary Sections 2 and 4.4).

Perturbing the system around its numerically obtained fixed-points, we constructed the Jacobian matrix  $J$  for each of our 20 systems. In Fig. 2 we find that, indeed, the diagonal and off-diagonal

terms of  $J$  follow the predicted scaling of (7) and (1.4). For example, in our Social model we predict  $\mu = 1$ , while our Regulatory dynamics are predicted to have  $\mu = 0$ , both scaling relationships clearly evident in Fig. 2a and c. This means that setting all diagonal terms to  $-C$ , as in May’s original formulation, misses the actual patterns that arise from the nonlinear Social/Regulatory dynamics. Similarly, the off-diagonal terms are proportional to  $k_i^{-1}k_j^0$  in Social (Fig. 2b) and  $k_i^0k_j^{-2}$  in Regulatory (Fig. 2d), again overruling the classic construction in which  $J_{ij}$  are extracted from an arbitrary  $P(w)$ . These scaling relationships, encapsulated within our analytically predicted  $\Omega$ , are independent of  $A_{ij}$  (SF1, SF2, SF3 or empirical), capturing the intrinsic, and most crucially, hitherto overlooked, contribution of the nonlinear dynamics to the structure of  $J$ .

Together, our analysis demonstrates that: (i) actual  $J$  matrices, extracted from real nonlinear dynamics are fundamentally distinct from random matrices; (ii) contrary to the random  $J$  ensembles, real Jacobians feature scaling patterns in which topology ( $P(k)$ ) and dynamics ( $\Omega$ ) are deeply intertwined; (iii) these patterns can be analytically traced to the system’s intrinsic nonlinear mechanisms ( $M_0(x), M_1(x), M_2(x)$ ) through Eqs. (7) and (1.4). Most crucially, while the random ensembles  $\mathbb{E}(P(w), C)$  and  $\mathbb{E}(A_{ij}, P(w), C)$  lead to the instability paradox of Eqs. (3) and (5), we show below that  $\mathbb{E}(A_{ij}, \Omega)$  has a much richer stability profile, in which a broad family of empirically relevant dynamics are predictably stable.

## Topology, dynamics and the emergence of stability

To address May’s paradox we analyze the  $\mathbb{E}(A_{ij}, \Omega)$  ensemble under a fat-tailed  $P(k)$ , as captured by Eq. (3.2). This setting allows us to observe the combined effect of dynamic nonlinearity ( $\Omega$ ) with one of the most ubiquitous features of real world networks, *i.e.* degree-heterogeneity<sup>4</sup>. In Supplementary Section 3 we show that extracting  $J$  from  $\mathbb{E}(A_{ij}, \Omega)$ , with a degree-heterogeneous  $A_{ij}$ , the principal eigenvalue asymptotically follows

$$\text{Re}(\lambda) \sim N^Q \left( 1 - \frac{C}{N^S} \right), \quad (9)$$

where  $Q$  and  $S$  depend both on network structure, through  $\beta$  in (3.2), and on the nonlinear dynamics via  $\Omega$ . Specifically, we show that

$$S = \beta(1 + \nu + \rho - \mu - \eta), \quad (10)$$

replacing the fixed exponents,  $1/2$  in (3), under  $\mathbb{E}(P(w), C)$ , and  $\beta/2$  in (5), under  $\mathbb{E}(A_{ij}, P(w), C)$ , with a variable exponent that depends on the dynamics-driven  $\Omega = (\eta, \mu, \nu, \rho)$ .

Equations (9) and (3.31) represent our key result. They show that, when extracted from real nonlinear dynamics of the form (1.1), the asymptotic behavior of  $\lambda$  is different from the one predicted in May’s original formulation, *i.e.* Eqs. (3) and (5). Most importantly, (9) and (3.31) have crucial implications regarding the system’s dynamic stability, distinguishing between three potential stability classes (Fig. 1f):

- **Asymptotic instability:**  $S > 0$  (red). In case  $S$  in (9) is positive, we have, for sufficiently large  $N$ ,  $\text{Re}(\lambda) \sim N^Q > 0$ . Such systems commit to the classic diversity-stability prediction, and, when large enough, become intrinsically unstable, regardless of the model parameters ( $C$ ). Specifically, setting  $\eta = \mu = \nu = \rho = 0$  we revert to the random matrix ensemble ( $\mathbb{E}(A_{ij}, P(w), C)$ ), for which  $S = \beta > 0$ , thus recovering May’s predicted instability. Hence, the diversity stability paradox is, indeed, a valid prediction, yet it represents

a specific point in a broader class of potential dynamic behaviors, driven by the parameter  $S$  in (3.31).

- **Asymptotic stability:**  $S < 0$  (blue). For a broad range of empirically relevant dynamics we have  $S < 0$ . Under these conditions, independently of  $C$ , the r.h.s. of (9) is dominated by the negative term, guaranteeing that  $\text{Re}(\lambda) < 0$ . Therefore, in this class, stability is not simply *enabled*, but rather, under  $N \rightarrow \infty$ , it becomes asymptotically inevitable, even if  $C \ll 1$ . Recalling May’s original question: *can a large complex system be stable?* - Eq. (9) with  $S < 0$  provides a clear answer: it not only *can*, but, in fact, *must* be stable.
- **Sensitive stability:**  $S = 0$  (green). Under  $S = 0$  the system lacks an asymptotic behavior, and therefore, its stability depends on  $C$  in (9). If  $C > 1$ , *i.e.* sufficiently strong negative feedback, the system is stable, otherwise it becomes unstable. As opposed to  $\Omega$ , which is intrinsic to the dynamic *model*, depending on the functional form of  $M_0(x), M_1(x), M_2(x)$  in (1.1),  $C$  is determined by the specific model *parameters*. Hence, in this class stability is not an intrinsic characteristic of the system, but rather it is sensitive to Eq. (1.1)’s tunable parameters.

This classification settles the debate on complex system stability on several levels. In the context of the diversity-stability paradox, it shows that large complex systems *can*, and in some cases even *must* be stable - hence reconciling between theory and empirical observation. More broadly, the stability classifier  $S$ , identifies the relevant topological ( $\beta$ ) and dynamic ( $\Omega$ ) control parameters that help analytically predict the stability class of any system within the form (1.1). We can therefore use  $S$  to predict *a priori* whether a specific combination of topology and dynamics will exhibit stable functionality or not.

To examine our stability classifier  $S$  we used our model and real networks to extract 2,077 Jacobian matrices from the  $\mathbb{E}(A_{ij}, \Omega)$  ensemble, with different sets of  $\eta, \mu, \nu$  and  $\rho$ . In Fig. 3a we show the principal eigenvalue  $\lambda$  vs.  $S$  for the entire 2,077 Jacobian sample. As predicted, we find that the parameter  $S$  sharply splits the sample into three classes. The asymptotically unstable class (red, top-right) has  $S > 0$  and consequently also  $\lambda > 0$ , a guaranteed instability. The asymptotically stable class (blue, bottom-left) is observed for  $S < 0$ , and has, in all cases  $\lambda < 0$ , as predicted. Finally, for  $S = 0$  we observe sensitive stability, with  $\lambda$  having no asymptotic positive/negative assignment (green). A small fraction ( $\sim 4\%$ ) of our sampled  $J$  matrices were inaccurately classified by  $S$  (grey), a consequence of the approximate nature of our derivations (Supplementary Section 3).

In Fig. 3a we also present the stability matrices associated with our empirical social, biological and ecological networks (symbols) examined earlier in Fig. 2. For each of these networks we constructed  $J$  via the  $\mathbb{E}(A_{ij}, P(w), C)$  ensemble, assigning random weights along the links, as well as via the  $\mathbb{E}(A_{ij}, \Omega)$  ensemble, with weights determined by (7) and (1.4), and  $\Omega$  taken according to the relevant dynamic model (Fig. 1g). While all these networks are classified unstable under the random ensemble (red symbols), as per May’s diversity-stability principle, once fit with  $J$  from our dynamic ensemble they all transition into the asymptotically stable class (blue symbols). *Hence, these empirical networks, when matched with real nonlinear interaction dynamics are, indeed, dynamically stable.*

Figures 2 and 3, together demonstrate our complete theoretical path: First, Fig. 2 shows that real  $J$  matrices exhibit the internal scaling patterns predicted in (7) and (1.4) - representing a steep departure from the broadly applied random matrix paradigm. Next, Fig. 3 shows that the resulting Jacobian ensemble has a rich space of potential dynamic behaviors, significantly

more diverse than the currently considered ensembles. Most importantly - this space contains a broad class ( $S \leq 0$ ) of asymptotically stable (blue) or sensitively stable (green) systems, that do not fall within May's paradox.

*Taken together, our analysis demonstrates that nature must not rely on devious strategies in order to ensure dynamic stability. The observed stability of large complex systems emerges quite naturally thanks to the built-in nonlinear interaction mechanisms between the system's components.*

## The ingredients of dynamic stability

The parameter  $S$  in (3.31) reduces a network's dynamic stability into five relevant exponents. The first four  $\Omega = (\eta, \mu, \nu, \rho)$  are determined by the nonlinear dynamics, Social, Regulatory, Ecological etc., and are therefore intrinsic to the system's inherent interaction mechanisms. These exponents are independent of the topology  $A_{ij}$  or of the microscopic model parameters, all of which are encapsulated within  $C$ . Therefore they are *hardwired* into the system's dynamic behavior. To understand this, consider, for example, our Social model, for which our formalism predicts  $\Omega = (0, 1, -1, 0)$  (Fig. 1g). This prediction is rooted in the SIS interaction mechanisms, *i.e.* infection vs. recovery, expressed through the functional form of  $M_0(x), M_1(x), M_2(x)$  of (1.1). It is, therefore, insensitive to the specific parameters of the model, *e.g.*, if the disease has a high or low infection rate, or if it is transmitted via physical contact or aerosols. Such distinctions, expressed through the model *parameters*, may impact the coefficient  $C$ , but do not affect  $\Omega$ , and therefore have no bearing on the stability classifier  $S$ . Hence,  $S$  is characteristic of, *e.g.*, the SIS *model*, not of its specific *parameters*.

The remaining exponent in (3.31),  $\beta$ , is independent of the dynamics, determined solely by  $A_{ij}$ , specifically by its degree distribution  $P(k)$ , through (3.2). This parameter quantifies the fat-tailed nature of  $P(k)$ , being  $\beta = 0$  for a bounded distribution, and approaching unity under extreme levels of degree-heterogeneity. Therefore, together,  $S$  captures the roles of both topology *and* dynamics, whose interplay determines the system's stability class - stable, unstable or sensitive.

**The role of degree-heterogeneity.** The prevalence of fat-tailed  $P(k)$  is among the defining features of real-world complex systems, from biological<sup>38</sup> to social<sup>16,17</sup> and technological<sup>41,42</sup> networks, with far-reaching implications on their observed dynamic behavior<sup>1,3,22</sup>. Our analysis indicates that this network characteristic may also play a crucial role in the context of dynamic stability. To understand this, consider a non fat-tailed  $P(k)$ , such as an Erdős-Rényi, network, where the degrees follow a Poisson distribution, having  $\beta = 0$ . Under these conditions we have  $S = 0$  in (3.31), the system has no defined asymptotic behavior, and hence it is sensitively stable - *i.e.* its stability depends on model parameters. Therefore, the existence of asymptotic stability/instability is a direct consequence of degree-heterogeneity, as, indeed, these forms of dynamic stability rely on  $\beta > 0$ .

This uncovers an additional layer to the dynamic impact of  $P(k)$  on complex system functionality. Consider, for example, the factors that drive a system towards the loss of stability. Most often such events result from external stress or changes in environmental conditions<sup>3</sup>. Such forces impact a system's functionality by perturbing its dynamic parameters, namely they affect  $C$ . Seldom, however, do these environmental perturbations affect the system's built-in interaction mechanisms. Indeed, while the dynamic mechanisms are fixed, ingrained in the *physics* of the interacting components, the specific model parameters often depend on external conditions.

The crucial point is, that under  $S < 0$ , a state only possible if  $P(k)$  is fat-tailed (*i.e.*  $\beta \neq 0$ ), stability becomes asymptotically independent on  $C$ , driven solely by  $\Omega$ , which is insensitive to specific model parameters. Hence, for a sufficiently large system ( $N \rightarrow \infty$ ), if  $P(k)$  is fat-tailed, stability becomes asymptotically robust against any external perturbation. *This suggests that degree-heterogeneity has evolved as a dynamically stabilizing topological characteristic, in the face of a persistently fluctuating environment.*

To illustrate this, consider again the SIS model (Social), for which  $\Omega = (0, 1, -1, 0)$ , and hence (3.31) predicts  $S = -\beta$ . Implemented on a scale-free network ( $\beta > 0$ ), Social has  $S < 0$ , and is thus asymptotically stable. However, the same dynamics on a bounded  $P(k)$  ( $\beta = 0$ ) becomes sensitively stable, and therefore its stability depends on the specific value of  $C$ , which can be tuned by changing the infection/recovery rates. Consequently, while generally Social's pandemic state is only stable if  $C > 1$ , in a scale-free environment it is *always* stable, even when  $C \rightarrow 0$ . This observation, predicted here directly from our formalism, recovers an already established result: the fact that in the SIS model, the epidemic threshold vanishes under a scale-free  $P(k)$ <sup>43</sup>. The crucial point is, however, that while the original result, particular to the SIS model, was obtained using a dedicated model-specific analysis, our control parameter  $S$  allows us to systematically analyze the stability profile of *all* combinations of topology/dynamics within (1.1), using a single universal classification.

To observe this role of  $P(k)$ , beyond the specific example of Social, we consider again  $\mathbb{E}(A_{ij}, \Omega)$ 's principal eigenvalue  $\lambda$  in (9). Its structure portrays stability as a balance between the positive, *i.e.* destabilizing, effect mediated by the network interactions, vs. the negative, stabilizing, feedback, driven by the parameter  $C$  in  $J$ 's diagonal (7), Fig. 3b-e. It is therefore, natural to enhance stability by increasing  $C$ , which, in effect, translates to strengthening each node's intrinsic negative feedback. Equation (9) predicts that a system becomes stable if  $C$  exceeds a critical value

$$C_0 \sim N^S, \quad (11)$$

beyond which  $\lambda$  becomes negative. For asymptotically stable systems ( $S < 0$ ) we have  $C_0 \rightarrow 0$ , a guaranteed stability even under arbitrarily small  $C$ . In contrast, for asymptotically unstable systems ( $S > 0$ ) we have  $C_0 \rightarrow \infty$ , hence such systems are impossible to stabilize even under extremely large  $C$ , *i.e.* extreme levels of negative feedback. The point is, that if  $P(k)$  is bounded we have, always,  $S = 0$  (sensitive stability), hence  $C_0$  is finite, and the system's stability can be controlled by tuning the parameter  $C$ , *e.g.*, changing the environmental conditions.

In Fig. 3c-k we extract again a set of three  $J$  matrices from  $\mathbb{E}(A_{ij}, \Omega)$ , representing systems from our three stability classes:  $J_{AS}$ , asymptotically stable with  $\Omega = (2, 2, 2, -1)$ ;  $J_{SS}$ , sensitively stable with  $\Omega = (0, -1, -2, 0)$ ; and  $J_{AU}$ , asymptotically unstable with  $\Omega = (1, -2, -1, 2)$ . For each of these we plot  $C_0$  vs.  $N$ , capturing the level of negative feedback required to ensure the system's stability. Under an Erdős-Rényi network, with bounded  $P(k)$  ( $\beta = 0$ ) we do not observe a defined asymptotic behavior. The critical  $C_0$  does not scale with  $N$ , indicating that sufficient perturbation to the model parameters can affect the system's stability (Fig. 3i-k, green circles).

The picture, however, fundamentally changes when we construct the same  $J$  matrices from a scale-free  $A_{ij}$  with  $\beta = 0.6$  (Fig. 3f-h), squares). Now we have  $S = -1.2, 0$  and  $1.8$  for  $J_{AS}$ ,  $J_{SS}$  and  $J_{AU}$ , respectively. As predicted in (11), under these condition, we observe a clear asymptotic

behavior, in which  $C_0$  scales with  $N$ . For  $J_{AS}$  we have  $C_0 \sim N^{-1.2}$ , while under  $J_{AU}$  we observe  $C_0 \sim N^{1.8}$  (solid lines), capturing the intrinsic stability/instability of these two systems. Finally, in  $J_{SS}$ , having  $S = 0$ , the system does not feature any asymptotic behavior, and therefore can be stabilized under finite  $C_0$ , independently of system size  $N$  (Fig. 3g). Hence, we observe a qualitative difference between bounded vs. scale-free  $P(k)$ , in which degree heterogeneity can potentially afford the network a guaranteed stability, that is asymptotically independent of microscopic parameters.

## Discussion

The linear stability matrix  $J$  carries crucial information on the dynamic behavior of a complex system. Here, we exposed distinct patterns in the structure of  $J$  that (i) arise from the nature of the system's interaction dynamics; (ii) affect its principal eigenvalue, and thus, its stability profile. These patterns are expressed through the four dynamic exponents  $\Omega = (\eta, \mu, \nu, \rho)$  in (7) and (1.4), linked analytically to the system's dynamics,  $M_0(x), M_1(x), M_2(x)$ , through the leading powers of the expansions in Eq. (1.63). This dependence on the *powers* ( $\Psi(n), \Gamma(n)$ , etc.), rather than the *coefficients* ( $G_n, C_n$ , etc.) indicates that  $\Omega$  is hardwired into the interaction dynamics. Indeed, the powers in (1.63) are determined by the dynamic model, *e.g.*, Social or Regulatory, but not the specific model parameters, which only impact the coefficients. Therefore, our predicted Jacobian ensemble in (7) and (1.4), as well as its associated stability classifier  $S$  in (3.31), both capture highly robust and distinctive characteristics of the system's dynamics, that cannot be perturbed or otherwise affected by shifting environmental conditions.

Graph spectral analysis represents a central mathematical tool to translate network structure into dynamic predictions<sup>44–46</sup>. A network's spectrum, *i.e.* its set of eigenvalues and eigenvectors, captures information on its dynamic time-scales, potential states, and - in the present context - its dynamic stability. *In that sense, the long-standing diversity-stability paradox exposed a severe and troubling clash between spectral graph theory and empirical observation. Here we reconcile this contradiction, by showing that, in effect, we have, all this time, been looking at the wrong spectrum.* Indeed, in its current application, spectral analysis is applied to the network *topology*, namely we seek the graph's eigenvalues. Focusing on the topology, however, loses information on the nonlinear dynamics that occur *on* that graph. Therefore, here, we offer to apply spectral analysis, not to the topology  $A_{ij}$ , but rather to the derived Jacobian in (7) and (1.4), which, thanks to  $\Omega$  preserves the information of both topology *and* dynamics.

In a broader perspective, the interplay between topology and dynamics is one of the major theoretical obstacles along the path to predict, understand and control complex system behavior<sup>47–50</sup>. The problem is that we lack sufficient theoretical tools to treat the ensuing combination of nonlinear dynamics with complex, random and often highly heterogeneous network structures. Consequently, advances are often system specific, requiring dedicated tools, and hence, lacking the breath of a general network dynamics theory. The Jacobian ensemble presented here, transforms the nonlinear Eq. (1.1) into an effective linear system, whose weights depend on both topology and dynamics. It can, therefore, allow us to utilize the powerful tools of spectral graph theory, even in a nonlinear dynamic setting. This may offer a basis for systematic analysis of nonlinear network dynamics.

**Data availability.** Upon acceptance, all codes/data to reproduce our analysis will be made available online.

### BOX I. THE ENSEMBLE $\mathbb{E}(A_{ij}, \Omega)$ - HOW TO CALCULATE $\Omega$

To construct  $J$  as appears in Eqs. (7) and (1.4) we must extract the exponents  $\Omega = (\eta, \mu, \nu, \rho)$  from Eq. (1.1). First we use the dynamic functions  $M_0(x), M_1(x)$  and  $M_2(x)$  to construct three new functions

$$R(x) = -\frac{M_1(x)}{M_0(x)}, \quad Y(x) = M_1(x)R'(x), \quad Z(x) = R(x)M_2(x), \quad (12)$$

where  $R'(x)$  represents a derivative  $dR/dx$  around the fixed point  $\mathbf{x}$ . From these we extract four additional functions, which we express through a Hahn power-series expansion as

$$\begin{aligned} M_2(Z^{-1}(x)) &= \sum_{n=0}^{\infty} G_n x^{\Psi(n)}, & Y(R^{-1}(x)) &= \sum_{n=0}^{\infty} C_n x^{\Gamma(n)}, \\ M_1(R^{-1}(x)) &= \sum_{n=0}^{\infty} K_n x^{\Pi(n)}, & M_2(R^{-1}(x)) &= \sum_{n=0}^{\infty} L_n x^{\Theta(n)} \end{aligned}, \quad (13)$$

where  $R^{-1}(x)$  and  $Z^{-1}(x)$  represent the inverse functions of  $R(x)$  and  $Z(x)$ . The Hahn expansion<sup>5</sup> is a generalization of the Taylor expansion to include negative and real powers. Hence  $\Psi(n), \Gamma(n), \Pi(n)$  and  $\Theta(n)$  represent series of real powers in ascending order, the leading (*i.e.* smallest) powers assigned the index  $n = 0$ . These leading powers directly provide  $\Omega$  via

$$\mu = 2 - \Gamma(0), \quad \nu = -\Pi(0), \quad \rho = -\Theta(0), \quad \eta = -\Psi(0)(\mu - \nu - \rho). \quad (14)$$

Hence, to construct  $J_{ij} \in \mathbb{E}(A_{ij}, \Omega)$  we first generate the network  $A_{ij}$ , then extract the degrees  $k_i$  of all nodes and the nearest neighbor degree  $\kappa_{\text{nn}}$ . The resulting  $J_{ij}$  satisfies

$$J_{ii} \sim -C \kappa_{\text{nn}}^{\eta} k_i^{\mu} \quad (15)$$

$$J_{ij} \sim A_{ij} k_i^{\nu} k_j^{\rho}, \quad (16)$$

where the constant  $C > 0$  captures the system's specific dynamic time-scales. Note that  $\Omega$ , as opposed to  $C$ , depends only on the leading *powers* of (1.63), and not on the *coefficients*. Therefore it is unaffected by Eq. (1.1)'s microscopic parameters, capturing an intrinsic characteristic of each dynamic model. The detailed derivation of  $\Omega$  appears in Supplementary Section 1, followed by a step by step application for all our dynamic models (Fig. 1g) in Supplementary Section 2.

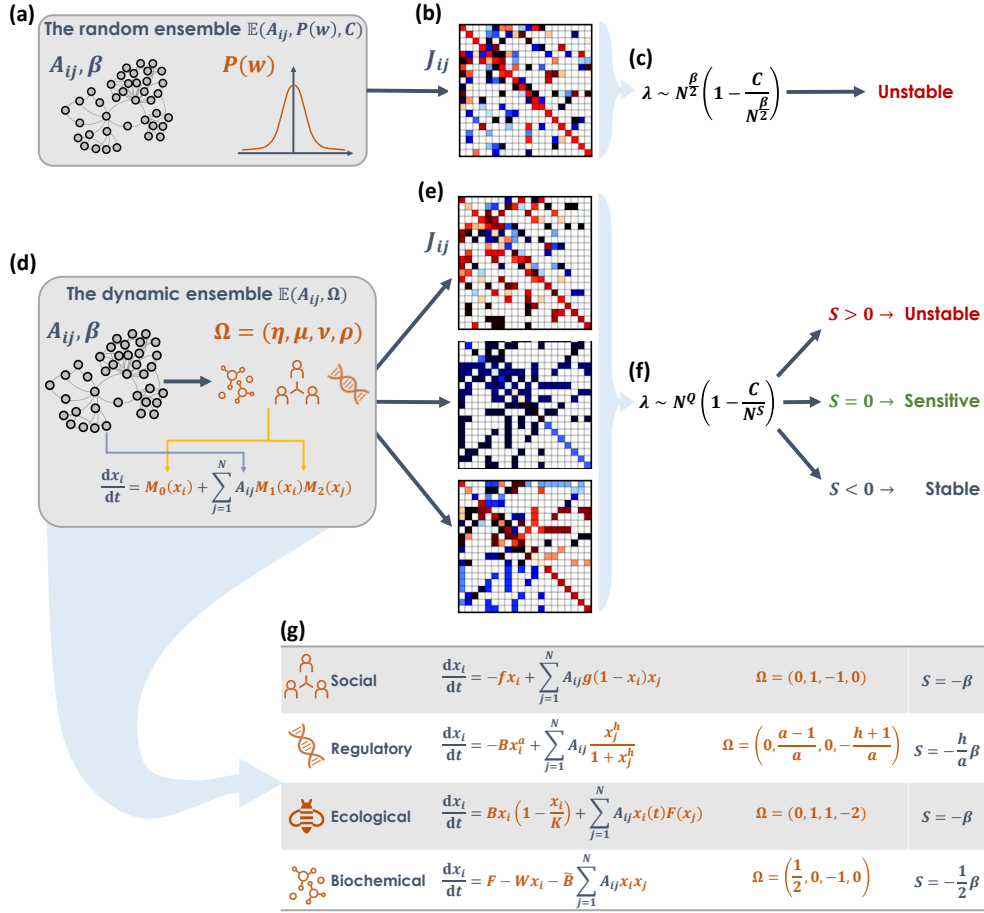


Figure 1: **Solving the diversity-stability paradox.** (a) A complex system is captured by an interaction network  $A_{ij}$ , whose diversity can be quantified by  $\beta$  in (3.2). In the random matrix framework, to assess its dynamic stability, we construct the system's Jacobian  $J$  with weights extracted independently from the distribution  $P(w)$ , and diagonal term set to  $-C$  (constant). (b) The resulting random stability matrix  $J_{ij}$ , belonging to the ensemble  $\mathbb{E}(A_{ij}, P(w), C)$ . (c) The principal eigenvalue, under this construction, diverges with the number of interacting components  $N$ , predicting that a large system *cannot* be stable. This non-realistic prediction captures the unresolved diversity-stability paradox. (d) Our alternative  $J$ -ensemble,  $\mathbb{E}(A_{ij}, \Omega)$ , is designed to capture the roles of both the network ( $A_{ij}, \beta$ , grey) and the nonlinear dynamic mechanisms of interaction, *e.g.*, Biochemical, Social or Regulatory (orange). These mechanisms are described by  $M_0(x), M_1(x), M_2(x)$  in Eq. (1.1), from which we extract the four exponents of  $\Omega$  (**Box I**). Here, the diagonal and off-diagonal weights of  $J_{ij}$  are not selected independently from  $P(w), C$ , but rather predicted by Eqs. (7) and (1.4). (e) As a result, the same  $A_{ij}$  may lead to different  $J$  matrices, as different dynamics are characterized by distinct  $\Omega$ . This captures the fact, absent in the random construction of (a)-(b), that the same network may exhibit diverse behaviors under different interaction mechanisms. (f) Consequently,  $\lambda$  follows a different form than in (c), with a variable *stability classifier*  $S$ , whose sign predicts the system's stability: Unstable (red) in which diversity, indeed, leads to instability; Sensitive (green), where diversity plays no role, and Stable (blue), in which diversity *enhances* stability. Hence, under real non-linear dynamics a large system *can* ( $S = 0$ ), and in some cases even *must* ( $S < 0$ ) be stable. (g) We use four common dynamic models capturing Social, Regulatory, Ecological and Biochemical interactions to examine our theoretical analysis. For each of these dynamics we extract  $\Omega$  and  $S$ , as detailed in Supplementary Section 2.

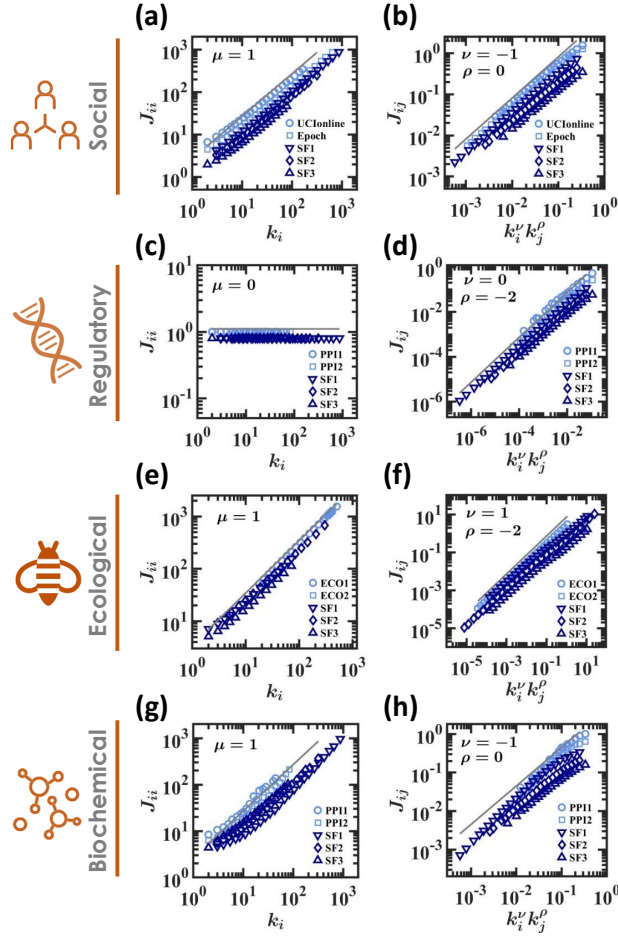


Figure 2: **Emerging patterns in the dynamic ensemble**  $\mathbb{E}(A_{ij}, \Omega)$ . We implemented Social, Regulatory, Ecological and Biochemical dynamics (Fig. 1g) on a set of relevant model (dark blue) and empirical (light blue) networks. Perturbing all nodes we numerically constructed each system's Jacobian,  $J$ , capturing *real* Jacobian matrices, as obtained from actual nonlinear dynamic models. (a) The diagonal terms  $J_{ii}$  vs. degree  $k_i$  as obtained from Social dynamics (symbols). We observe the scaling relationship of Eq. (7) with  $\mu = 1$  (solid line) confirming our predicted scaling for this dynamics. (b) The off diagonal terms  $J_{ij}$  vs. prediction (1.4) with  $\nu = -1, \rho = 0$  (symbols). Once again, we observe a perfect agreement with our theoretical prediction (solid line). We also include results obtained from two relevant empirical networks, Epoch<sup>17</sup> and UCInonline<sup>16</sup>, capturing online social dynamics. (c) - (d) Similar results are observed under Regulatory dynamics ( $\mu = \nu = 0, \rho = -2$ ) on both the model and the real networks (PPI1<sup>18</sup> and PPI2<sup>19</sup>); (e) - (f) Ecological dynamics ( $\mu = \nu = 1, \rho = -2$ ), using the real networks ECO1 and ECO2<sup>22</sup>; (g) - (h) Biochemical dynamics ( $\mu = 1, \nu = -1, \rho = 0$ ). As predicted, we find that real Jacobian matrices exhibit the non-random patterns of Eqs. (7) and (1.4), and therefore cannot be modeled via the random ensemble  $\mathbb{E}(A_{ij}, P(w), C)$ , but rather through our offered dynamic Jacobian family  $\mathbb{E}(A_{ij}, \Omega)$ . Data in all panels are logarithmically binned<sup>14</sup>. Details on the numerical calculation of  $J$ , log-binning and the construction of the networks all appear in Supplementary Section 4.

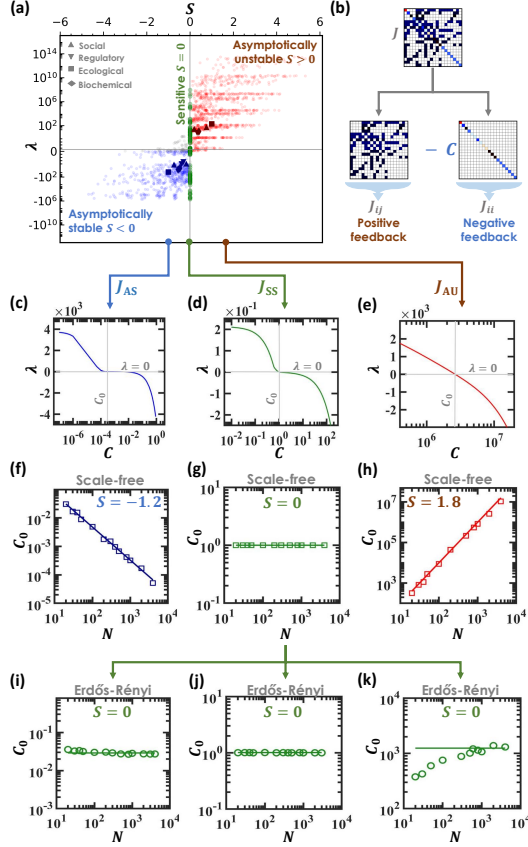


Figure 3: **Three classes of dynamic stability in real and model networks.** We extracted 2,077 Jacobian matrices from the  $\mathbb{E}(A_{ij}, \Omega)$  ensemble, using combinations of model/real networks with different dynamic exponents  $\Omega$ . For each  $J$  we calculated the principal eigenvalue  $\lambda$  and the stability classifier  $S$  in (3.31). (a)  $\lambda$  vs.  $S$  for all 2,077  $J$ -matrices. We observe the three predicted classes: Asymptotically unstable (red) in which  $S > 0$  and hence also  $\lambda > 0$ ; Sensitively stable (green), where  $S = 0$  and  $\lambda$  can be both positive or negative; Asymptotically stable (blue), where  $S < 0$  and therefore  $\lambda < 0$ . Our classification was inaccurate in  $\sim 4\%$  of the cases (grey). Empirical networks (solid symbols): Under the random ensemble  $\mathbb{E}(A_{ij}, P(w), C)$  all our empirical networks are classified as unstable (red symbols). However, the same networks under  $\mathbb{E}(A_{ij}, \Omega)$ , each with its relevant  $\Omega$ , become dynamically stable (blue symbols). This exemplifies the importance of the topology/dynamics interplay, as networks rendered unstable via the existing paradigm, are, in fact, stable, when the nonlinearity is correctly implemented through  $\Omega$ . (b) The value of  $\lambda$  emerges from the competition between the diverse interactions (off diagonal terms  $J_{ij}$ , positive feedback) and the strength of the diagonal terms  $J_{ii}$  (negative feedback). Hence one can force a system towards stability ( $\lambda < 0$ ) by increasing  $C$  in (7). (c) - (e) Taking three specific  $J$  matrices from each class, we plot  $\lambda$  vs.  $C$ , seeking the critical  $C_0$ , in which  $\lambda$  becomes negative (grey lines). (f) For the stable  $J_{AS}$  ( $S = -1.2$ ) we find that  $C_0$  decreases with  $N$  (squares), capturing the asymptotic stability, in which for large systems ( $N \rightarrow \infty$ ) stability is sustained even under arbitrarily small  $C$ . The theoretical scaling predicted in Eq. (11) is also shown (solid line, slope  $-1.2$ ). (g) For  $J_{SS}$ , in the sensitively stable class  $S = 0$ , the critical  $C_0$  is independent of  $N$ , hence the system's stability can be affected by finite changes to its dynamic parameters, *e.g.*, through environmental perturbations. (h) The asymptotically unstable  $J_{AU}$  ( $S = 1.8$ ) has  $C_0 \rightarrow \infty$  in the limit of large  $N$ , in perfect agreement with (11), solid line. (i) - (k) For a bounded  $P(k)$ , *e.g.*, Erdős-Rényi,  $\beta$  vanishes and hence  $S = 0$  in (3.31). Under these conditions, regardless of  $\Omega$ , the system is sensitively stable and therefore  $C_0$  does not scale with  $N$ . This demonstrates the role of degree-heterogeneity in ensuring stability, in the face of changing environmental conditions.

## References

- [1] S.V. Buldyrev, R. Parshani, G. Paul, H.E. Stanley and S. Havlin. Catastrophic cascade of failures in interdependent networks. *Nature*, 464:1025–1028, 2010.
- [2] I. Dobson, B.A. Carreras, V.E. Lynch and D.E. Newman. Complex systems analysis of series of blackouts: Cascading failure, critical points, and self-organization. *Chaos*, 17:026103, 2007.
- [3] D. Duan, C. Lv, S. Si, Z. Wang, D. Li, J. Gao, S. Havlin, H.E. Stanley and S. Boccaletti. Universal behavior of cascading failures in interdependent networks. *Proc. Natl. Acad. Sci. USA*, 116:22452–57, 2019.
- [4] A.E. Motter and Y.-C. Lai. Cascade-based attacks on complex networks. *Physical Review E*, 66:065102, 2002.
- [5] P. Crucitti, V. Latora and M. Marchiori. Model for cascading failures in complex networks. *Phys. Rev. E*, 69:045104–7, 2004.
- [6] D. Achlioptas, R.M. D’Souza and J. Spencer. Explosive percolation in random networks. *Science*, 323:1453–1455, 2009.
- [7] J. Gao, B. Barzel and A.-L. Barabási. Universal resilience patterns in complex networks. *Nature*, 530:307–312, 2016.
- [8] S. Boccaletti, J.A. Almendral, S. Guana, I. Leyvad, Z. Liua, I.S. Nadal, Z. Wang and Y. Zou. Explosive transitions in complex networks structure and dynamics: Percolation and synchronization. *Physics Reports*, 660:1–94, 2016.
- [9] S. Boccaletti, V. Latora, Y. Moreno, M. Chavez and D.-U. Hwang. Complex networks: Structure and dynamics. *Physics Reports*, 424:175–308, 2006.
- [10] R. Cohen and S. Havlin. Scale-free networks are ultrasmall. *Phys. Rev. Lett.*, 90:058701–4, 2003.
- [11] K.Z. Coyte<sup>1</sup>, J. Schluter<sup>1</sup> and K.R. Foster<sup>1</sup>. The ecology of the microbiome: Networks, competition, and stability. *Science*, 350:663–666, 2015.
- [12] D. Tilman, P.B. Reich and J.M.H. Knops. Biodiversity and ecosystem stability in a decade-long grassland experiment. *Nature*, 441:629632, 2006.
- [13] R.V. Solé and J.M. Montoya. Complexity and fragility in ecological networks. *Proc. R. Soc. London Ser. B*, 268:2039–2045, 2001.
- [14] R.M. May. Will a large complex system be stable? *Nature*, 238:413 – 414, 1972.
- [15] G. Caldarelli. *Scale-free networks: complex webs in nature and technology*. Oxford University Press, New York, 2007.
- [16] A.-L. Barabási, H. Jeong, E. Ravasz, Z. Néda, A. Schubert and T. Vicsek. *Physica A*, 311:590, 2002.
- [17] D.J. Watts and S.H. Strogatz. Collective dynamics of ‘small-world’ networks. *Nature*, 393:440–442, 1998.

- [18] B. Barzel and O. Biham. Quantifying the connectivity of a network: The network correlation function method. *Phys. Rev. E*, 80:046104–15, 2009.
- [19] A.-L. Barabási and R. Albert. Emergence of scaling in random networks. *Science*, 286:509–512, 1999.
- [20] M.E.J. Newman. *Networks - an introduction*. Oxford University Press, New York, 2010.
- [21] S. Allesina and S. Tang. Stability criteria for complex ecosystems. *Nature*, 483:205208, 2012.
- [22] G. Yan, N.D. Martinez and Y.-Y. Liu. Degree heterogeneity and stability of ecological networks. *Journal of The Royal Society Interface*, 14:131, 2017.
- [23] C. Jacquet, C. Moritz, L. Morissette, P. Legagneux, F. Massol, P. Archambault and D. Gravel. No complexity-stability relationship in empirical ecosystems. *Nature Communications*, 7:12573, 2016.
- [24] B. Barzel and A.-L. Barabási. Universality in network dynamics. *Nature Physics*, 9:673 – 681, 2013.
- [25] U. Harush and B. Barzel. Dynamic patterns of information flow in complex networks. *Nature Communications*, 8:2181, 2017.
- [26] C. Hens, U. Harush, R. Cohen, S. Haber and B. Barzel . Spatiotemporal propagation of signals in complex networks. *Nature Physics*, 15:403, 2019.
- [27] R. Pastor-Satorras, C. Castellano, P. Van Mieghem and A. Vespignani. Epidemic processes in complex networks. *Rev. Mod. Phys.*, 87:925–958, 2015.
- [28] P.S. Dodds, R. Muhamad and D.J. Watts. An experimental study of search in global social networks. *Science*, 301:827–829, 2003.
- [29] D. Brockmann, V. David and A.M. Gallardo. Human mobility and spatial disease dynamics. *Reviews of Nonlinear Dynamics and Complexity*, 2:1, 2009.
- [30] G. Karlebach and R. Shamir. Modelling and analysis of gene regulatory networks. *Nature Reviews*, 9:770–780, 2008.
- [31] J.D. Murray. *Mathematical Biology*. Springer, Berlin, 1989.
- [32] B. Barzel and O. Biham. Binomial moment equations for stochastic reaction systems. *Phys. Rev. Lett.*, 106:150602–5, 2011.
- [33] B. Barzel and O. Biham. Stochastic analysis of complex reaction networks using binomial moment equations. *Phys. Rev. E*, 86:031126, 2012.
- [34] C.S. Holling. Some characteristics of simple types of predation and parasitism. *The Canadian Entomologist*, 91:385–398, 1970.
- [35] J.N. Holland, D.L. DeAngelis and J.L. Bronstein. Population dynamics and mutualism: functional responses of benefits and costs. *American Naturalist*, 159:231–244, 2002.

- [36] E.L. Berlow, J.A. Dunne, N.D. Martinez, P.B. Stark, R.J. Williams and U. Brose. Simple prediction of interaction strengths in complex food webs. *Proceedings of the National Academy of Sciences*, 106:187–191, 2009.
- [37] J.F. Hayes and T.V.J. Ganesh Babu. *Modeling and Analysis of Telecommunications Networks*. John Wiley & Sons, Inc., Hoboken, NJ, USA, 2004.
- [38] A.-L. Barabási and Z.N. Oltvai. Network biology: understanding the cell’s functional organization. *Nat. Rev. Gen.*, 5:101, 2004.
- [39] T. Opsahl and P. Panzarasa. Clustering in weighted networks. *Social Networks*, 31:155–163, 2009.
- [40] J.-P. Eckmann, E. Moses and D. Sergi. Entropy of dialogues creates coherent structures in e-mail traffic. *Proc. Natl. Acad. Sci. USA*, 101:14333–7, 2004.
- [41] M. Faloutsos, P. Faloutsos and C. Faloutsos. On power-law relationships of the Internet topology. *Comput. Commun. Rev.*, 29:251–262, 1999.
- [42] G. Caldarelli and M. Catanzaro. *Networks: A very short introduction*. Oxford University Press, New York, 2012.
- [43] M. Boguñá, R. Pastor-Satorras and A. Vespignani. Absence of epidemic threshold in scale-free networks with degree correlations. *Phys. Rev. Lett.*, 90:028701–4, 2003.
- [44] J.A. Almendral and A. Díaz-Guilera. Dynamical and spectral properties of complex networks. *New Journal of Physics*, 9:187–187, 2007.
- [45] P. Van Mieghem. Epidemic phase transition of the SIS type in network. *Europhysics Letters*, 97(4):48004, 2012.
- [46] P. Van Mieghem. *Graph Spectra for Complex Networks*. Cambridge University Press, Cambridge, UK, 2010.
- [47] V.S. Afraimovich and L.A. Bunimovich. Dynamical networks: interplay of topology, interactions and local dynamics. *Nonlinearity*, 20:1761–1771, 2007.
- [48] C. Kirst, M. Timme and D. Battaglia. Dynamic information routing in complex networks. *Nature Communications*, 7:11061, 2016.
- [49] A. Barrat, M. Barthélemy and A. Vespignani. *Dynamical Processes on Complex Networks*. Cambridge University Press, Cambridge, 2008.
- [50] G. Yan, G. Tsekenis, B. Barzel, J.-J. Slotine, Y.-Y. Liu and A.-L. Barabási. Spectrum of controlling and observing complex networks. *Nature Physics*, 11:779786, 2015.
- [51] L. Schmetterer and K. Sigmund (Eds.). *Hans Hahn Gesammelte Abhandlungen Band 1/Hans Hahn Collected Works Volume 1*. Springer, Vienna, Austria, 1995.
- [52] H. Yu *et al.* High-quality binary protein interaction map of the yeast interactome network. *Science*, 322:104–110, 2008.
- [53] J.F. Rual *et al.* Towards a proteome-scale map of the human protein-protein interaction network. *Nature*, 437:1173–1178, 2005.

- [54] Interaction web database. <http://www.nceas.ucsb.edu/interactionweb/resources>.
- [55] S. Milojević. Power-law distributions in information science: making the case for logarithmic binning. *Journal of the American Society for Information Science and Technology*, 61:2417–2425, 2010.

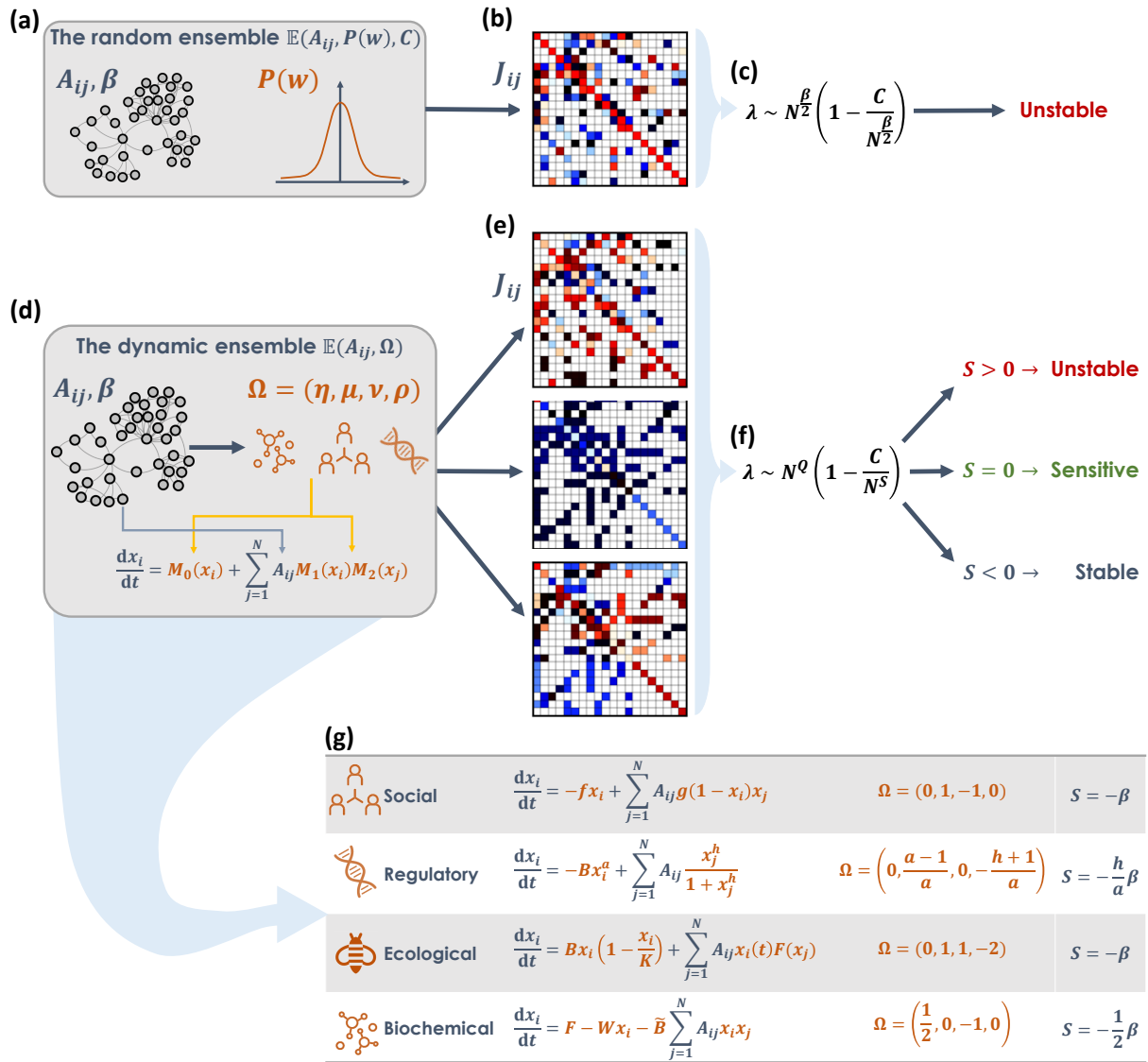


Figure 1 - full size.

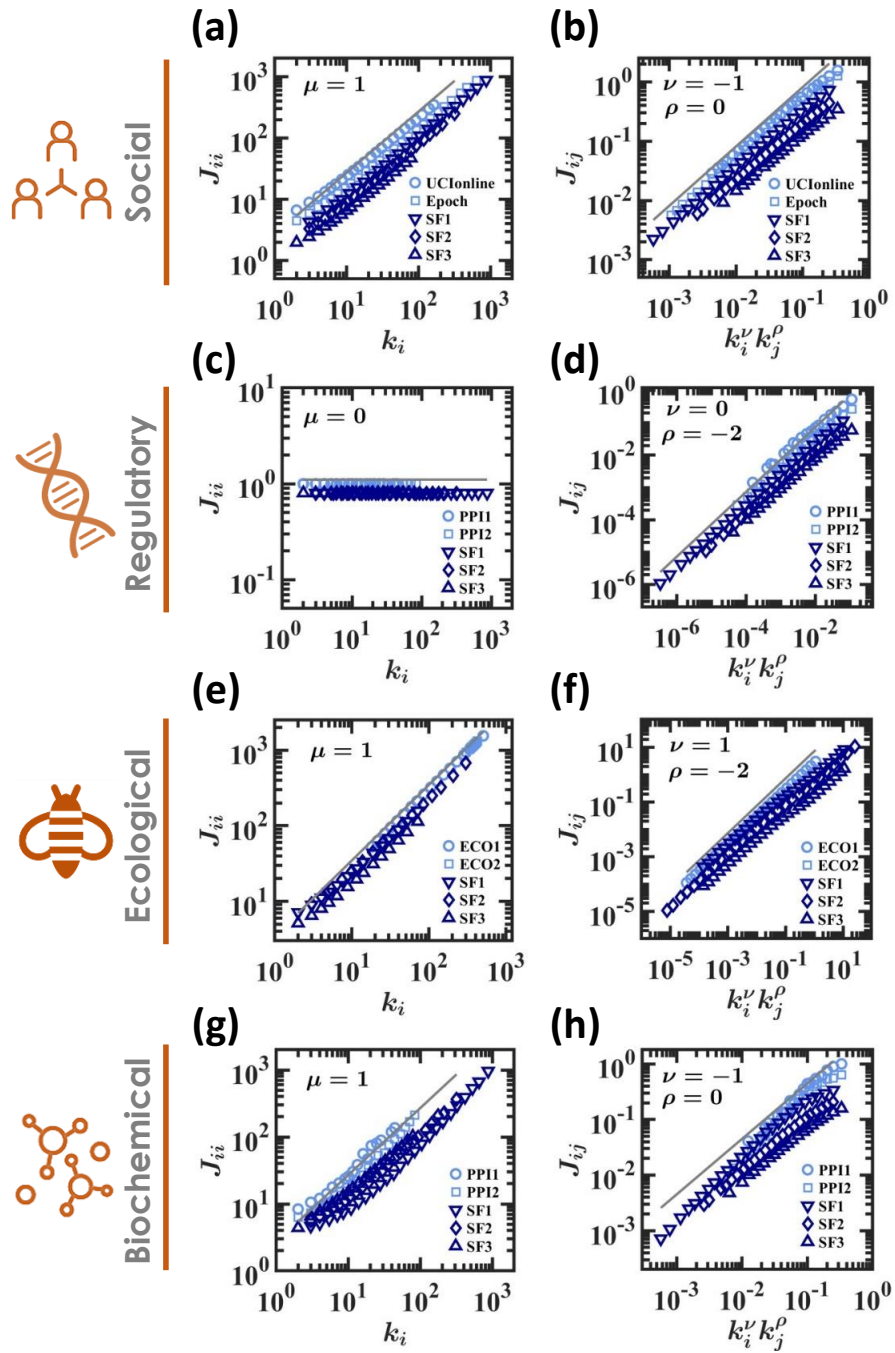


Figure 2 - full size.

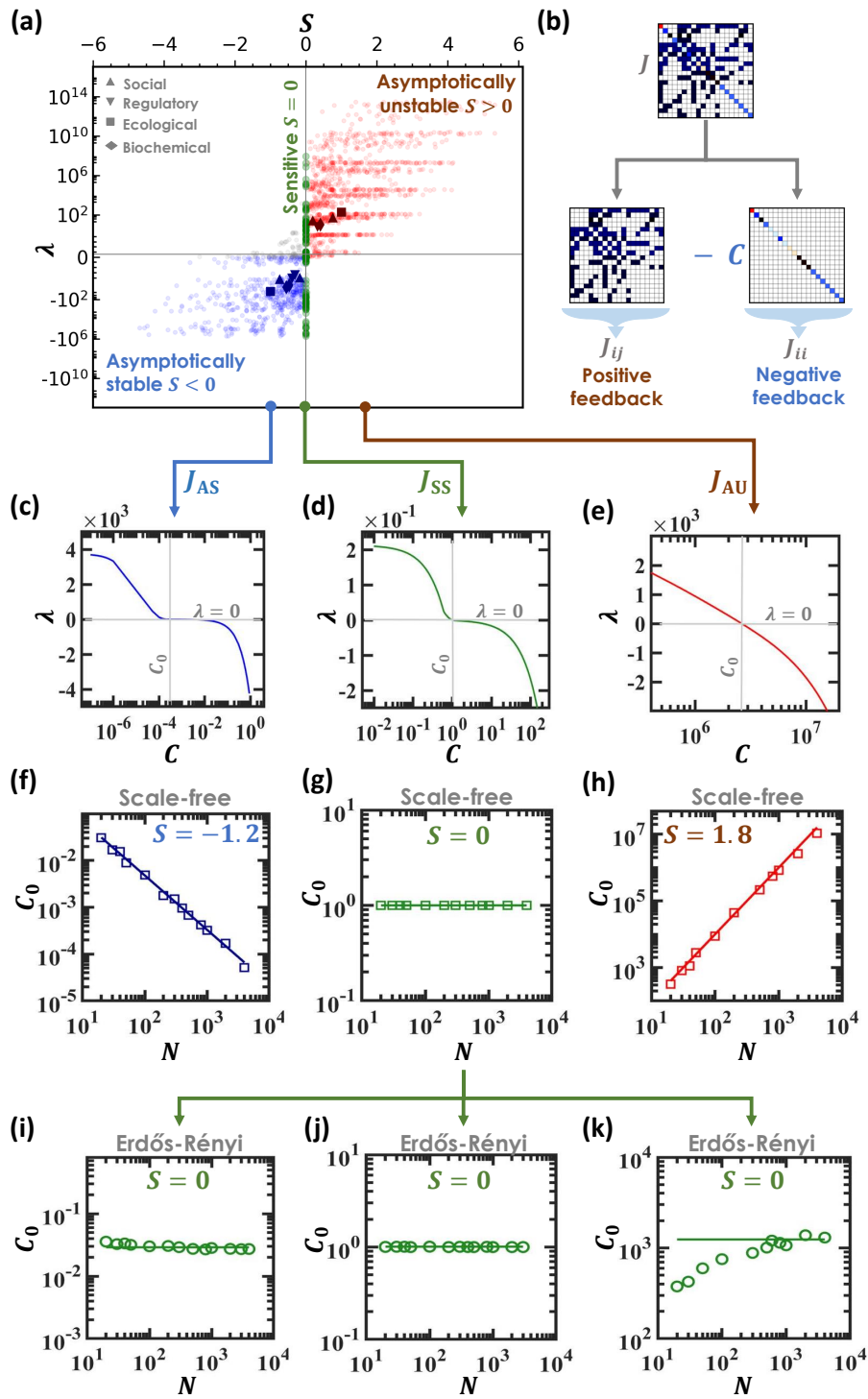


Figure 3 - full size.

# Dynamic stability of complex networks - Supplementary information

July 26, 2022

# Contents

|          |   |           |
|----------|---|-----------|
| <b>1</b> | <b>The Jacobian ensemble <math>\mathbb{E}(A_{ij}, \Omega)</math></b>              | <b>1</b>  |
| 1.1      | The fixed-points $\mathbf{x}^*$ . . . . .   | 1         |
| 1.1.1    | Evaluating $\langle M_2(x) \rangle_{\odot}$ . . . . .                             | 3         |
| 1.2      | Diagonal terms $D_{ii}$ . . . . .   | 5         |
| 1.3      | The off-diagonal terms $W_{ij}$ . . . . .   | 6         |
| 1.4      | Piecing together the $J_{ij}$ puzzle . . . . .                                    | 8         |
| 1.4.1    | Impact of $P(k)$ and $\kappa_{\text{nn}}$ . . . . .                               | 9         |
| <b>2</b> | <b>Analyzing the dynamic models</b>   | <b>12</b> |
| 2.1      | Social dynamics . . . . .   | 12        |
| 2.2      | Regulatory dynamics . . . . .   | 13        |
| 2.3      | Ecological dynamics . . . . .   | 15        |
| 2.4      | Biochemical dynamics . . . . .  | 16        |
| <b>3</b> | <b>Principle eigenvalue of <math>J_{ij} \in \mathbb{E}(A_{ij}, \Omega)</math></b> | <b>18</b> |
| 3.1      | The role of topology vs. dynamics . . . . .                                       | 23        |
| <b>4</b> | <b>Methods and data analysis</b>  | <b>23</b> |
| 4.1      | Numerical integration . . . . .   | 23        |
| 4.2      | Numerically estimating $J_{ij}$ . . . . .   | 24        |
| 4.3      | Logarithmic binning . . . . .   | 24        |
| 4.4      | Model and empirical networks . . . . .  | 25        |

# 1 The Jacobian ensemble $\mathbb{E}(A_{ij}, \Omega)$

To analyze complex system stability we seek the *real* Jacobian matrix  $J_{ij}$ , as extracted from the system's specific nonlinear interaction mechanisms. We first rewrite Eq. (6) of the main text as

$$\frac{dx_i}{dt} = F_i(\mathbf{x}(t)), \quad (1.1)$$

where

$$F_i(\mathbf{x}(t)) = M_0(x_i(t)) + \sum_{j=1}^N A_{ij} M_1(x_i(t)) M_2(x_j(t)). \quad (1.2)$$

We denote (1.1)'s fixed-point(s) by  $\mathbf{x}^* = (x_1, \dots, x_N)^\top$ , where we omit the term  $t$  to capture their independence on time. These fixed-points are obtained by solving the equilibrium equation

$$F_i(\mathbf{x}^*) = 0. \quad (1.3)$$

To assess the dynamic stability of each solution we track its response to small perturbations, via the Jacobian

$$J_{ij} = \left. \frac{\partial F_i(\mathbf{x})}{\partial x_j} \right|_{\mathbf{x}=\mathbf{x}^*}, \quad (1.4)$$

whose structure we obtain below. Writing

$$J = A \otimes W - I \otimes D \quad (1.5)$$

we treat separately the diagonal terms  $J_{ii} = D_{ii}$  and the off-diagonal terms  $J_{ij} = A_{ij} W_{ij}$  ( $I$  is the identity matrix and  $\otimes$  is the Hadamard product).

## 1.1 The fixed-points $\mathbf{x}^*$

We consider systems of the form (1.1) that exhibit at least one fully positive fixed-point  $\mathbf{x}^*$ . Using Eq. (1.3) we write

$$M_0(x_i) + \sum_{j=1}^N A_{ij} M_1(x_i) M_2(x_j) = 0, \quad (1.6)$$

which can be expressed as

$$R(x_i) \sum_{j=1}^N A_{ij} M_2(x_j) = 1, \quad (1.7)$$

where

$$R(x_i) = -\frac{M_1(x_i)}{M_0(x_i)}. \quad (1.8)$$

Denoting  $i$ 's degree by  $k_i = \sum_{j=1}^N A_{ij}$  we write (1.7) as

$$R(x_i) = \frac{1}{k_i \langle M_2(x) \rangle_{i, \odot}}, \quad (1.9)$$

in which

$$\langle M_2(x) \rangle_{i, \odot} = \frac{1}{k_i} \sum_{j=1}^N A_{ij} M_2(x_j) \quad (1.10)$$

represents an average of the function  $M_2(x_j)$  over all of node  $i$ 's direct network *neighborhood*, which we captured by the  $\odot$  symbol. Assuming the function  $R(x)$  is invertible around  $x_i$  we obtain  $i$ 's fixed-point activity as

$$x_i = R^{-1}(q_i), \quad (1.11)$$

where  $R^{-1}(x)$  is the inverse function of  $R(x)$  and

$$q_i = \frac{1}{k_i \langle M_2(x) \rangle_{i, \odot}}. \quad (1.12)$$

is  $i$ 's inverse degree, which approaches zero in the limit of large  $k_i$ .

To understand the dependence of activity on degree, we seek the average steady-state activity over all nodes with degree  $k$  as

$$x(k) = \frac{1}{|\mathbf{G}(k)|} \sum_{i \in \mathbf{G}(k)} x_i, \quad (1.13)$$

where  $\mathbf{G}(k) = \{i \in [1, N] | k_i = k\}$  is the group of all nodes with degree  $k$ , and  $|\mathbf{G}(k)|$  is the number of nodes in that group. To approximate  $x(k)$  we first evaluate the average neighborhood activity of all nodes in  $\mathbf{G}(k)$  via

$$\langle M_2(x) \rangle_{k, \odot} = \frac{1}{|\mathbf{G}(k)|} \sum_{i \in \mathbf{G}(k)} \langle M_2(x) \rangle_{i, \odot}, \quad (1.14)$$

capturing the typical value of  $M_2(x)$  surrounding nodes with degree  $k$ . Most generally, the activities  $x_j$  may depend, to some extent, on the degree  $k_i$  of their neighbor  $i$ , however this dependence is often unknown, and, most importantly, relatively weak<sup>1</sup>. Indeed,  $i$  is but one of  $j$ 's  $k_j$  neighbors, who are typically a random selection, representative of the network's degree distribution<sup>2</sup>. Therefore,  $i$ 's degree  $k_i$  is only weakly correlated with  $j$ 's activity  $x_j$ . To capture this dependence we approximate (1.14) as

$$\langle M_2(x) \rangle_{k, \odot} \approx f(k) \langle M_2(x) \rangle_{\odot}, \quad (1.15)$$

where

$$\langle M_2(x) \rangle_{\odot} = \frac{1}{N} \sum_{i=1}^N \frac{1}{k_i} \sum_{j=1}^N A_{ij} M_2(x_j) \quad (1.16)$$

represents the average of the function  $M_2(x_j)$  over *all* network neighborhoods, independent of  $i$  or  $k$ . In (1.15) the term  $\langle M_2(x) \rangle_{\odot}$  captures a characteristic aggregated function of the system's fixed-point, capturing the value of  $M_2(x_j)$  averaged over all nearest neighbor nodes, but not specifically over  $i$ 's neighbors - hence the approximation sign  $\approx$ , rather than  $=$ . The function  $f(k)$  corrects this average to account for the fact that in the l.h.s. of (1.15) the average is carried out selectively over nodes whose neighbor has degree  $k$ . For example,  $f(k) = 1$  represents the *perfect* case of no degree-correlations, under which  $x_j$  is fully independent of its neighbor's degree  $k$ . More generally, we assume  $f(k)$  to be a *weak* function, *i.e.* sub-polynomial in  $k$ , for example

$$f(k) \sim \log^n(k). \quad (1.17)$$

We can now approximate  $x(k)$  in (1.13), taking  $x_i$  from (1.11), and  $\langle M_2(x) \rangle_{i,\odot}$  from (1.15) to obtain

$$x(k) = R^{-1}(q), \quad (1.18)$$

where

$$q = \frac{1}{f(k) \langle M_2(x) \rangle_{\odot} k}. \quad (1.19)$$

In the asymptotic limit of large  $k$ , the sub-polynomial contribution of  $f(k)$  becomes negligible, and hence we have

$$q \sim \langle M_2(x) \rangle_{\odot}^{-1} k^{-1}. \quad (1.20)$$

### 1.1.1 Evaluating $\langle M_2(x) \rangle_{\odot}$

To link  $\langle M_2(x) \rangle_{\odot}$  to the network  $A_{ij}$  we use a mean-field approximation. We first define the nearest neighbor activity as

$$x_{\text{nn}} = \langle x \rangle_{\odot} = \frac{1}{N} \sum_{i=1}^N \frac{1}{k_i} \sum_{j=1}^N A_{ij} x_j, \quad (1.21)$$

and its corresponding nearest neighbor degree as

$$\kappa_{\text{nn}} = \langle k \rangle_{\odot} = \frac{1}{N} \sum_{i=1}^N \frac{1}{k_i} \sum_{j=1}^N A_{ij} k_j. \quad (1.22)$$

Hence, the average nearest neighbor node is characterized by activity  $x_{\text{nn}}$  and degree  $\kappa_{\text{nn}}$ . While  $x_{\text{nn}}$  depends on the system's dynamics (1.1),  $\kappa_{\text{nn}}$  is fully determined by the topology  $A_{ij}$ , linked to the network's degree distribution  $P(k)$ . Specifically we have<sup>3</sup>

$$\kappa_{\text{nn}} = \frac{\langle k^2 \rangle}{\langle k \rangle}, \quad (1.23)$$

with  $\langle k^n \rangle$  capturing the  $n$ th moment of  $P(k)$ . For a homogeneous network in which  $P(k)$  is bounded we have  $\kappa_{\text{nn}} \approx \langle k \rangle$ , however, if the network is highly heterogeneous, *i.e.*  $P(k)$  is fat-tailed - as indeed, many real networks are<sup>4</sup> - we find that  $\kappa_{\text{nn}} \gg \langle k \rangle$ , in extreme cases even diverging with system size as  $\kappa_{\text{nn}} \sim N^\beta$ .

We can now link  $\langle M_2(x) \rangle_{\odot}$  in (1.16) to  $\kappa_{\text{nn}}$  and  $x_{\text{nn}}$ , as, indeed,  $\langle M_2(x) \rangle_{\odot}$  is designed to capture the mean value of  $M_2(x)$  over all nearest neighbor nodes, namely nodes with typical degree  $\kappa_{\text{nn}}$  and activity  $x_{\text{nn}}$ . We, therefore, we approximate (1.16) as

$$\langle M_2(x) \rangle_{\odot} \approx M_2(x_{\text{nn}}), \quad (1.24)$$

in which we swap the order of operations from  $\langle M_2(x) \rangle$  to  $M_2(\langle x \rangle)$ . Such approximation becomes exact in the limit where  $M_2(x)$  is linear or when  $x_j$  are narrowly distributed. It is also justified when  $M_2(x)$  is sub-linear, *e.g.*, a saturating function  $M_2(x \rightarrow \infty) \rightarrow 1$ . Under these conditions, even if  $x_j$  are broadly distributed,  $M_2(x_j)$  are more uniform, and hence their average is (roughly) concentrated around  $M_2(\langle x \rangle)$ . For a super-linear  $M_2(x)$ , and under broadly distributed  $x_j$ , however, approximation (1.24) becomes inaccurate.

To evaluate  $M_2(x_{\text{nn}})$ 's dependence on  $\kappa_{\text{nn}}$  we use (1.9) to write

$$R(x_{\text{nn}}) = \frac{1}{\kappa_{\text{nn}} f(\kappa_{\text{nn}}) M_2(x_{\text{nn}})}, \quad (1.25)$$

where we substitute  $\langle M_2(x) \rangle_{i,\odot}$  by  $f(\kappa_{\text{nn}}) M_2(x_{\text{nn}})$  following approximations (1.15) and (1.24), and use the nearest neighbor degree  $\kappa_{\text{nn}}$  in place of  $k$ . We therefore arrive at

$$Z(x_{\text{nn}}) = \frac{1}{f(\kappa_{\text{nn}}) \kappa_{\text{nn}}} \equiv q_{\odot}, \quad (1.26)$$

where  $Z(x) = R(x) M_2(x)$  is a dynamic function, fully determined by  $M_0(x)$ ,  $M_1(x)$  and  $M_2(x)$  in (1.1). In (1.27) we use the notation  $q_{\odot}$  to signify the inverse degree ( $q$ ) associated with the typical *neighborhood* ( $\odot$ ). By inversion we obtain

$$x_{\text{nn}} = Z^{-1}(q_{\odot}), \quad (1.27)$$

and hence

$$M_2(x_{\text{nn}}) = M_2(Z^{-1}(q_{\odot})). \quad (1.28)$$

To obtain the asymptotic scaling of  $M_2(x_{\text{nn}})$  on  $\kappa_{\text{nn}}$  we use the Hahn expansion<sup>5</sup> to express  $Z(x)$  in the form of a power series around  $q_{\odot} \rightarrow 0$ , *i.e.*  $\kappa_{\text{nn}} \rightarrow \infty$ . Hence we write

$$M_2(Z^{-1}(q_{\odot})) = \sum_{n=0}^{\infty} G_n q_{\odot}^{\Psi(n)}, \quad (1.29)$$

where  $\Psi(n)$  is a set of real powers in ascending order with  $n$ . In the limit of large  $\kappa_{\text{nn}}$  (small

$q_{\odot}$ ) the expansion in (1.29) is dominated by the leading power  $\Psi(0)$ , predicting that

$$M_2(x_{\text{nn}}) \sim \kappa_{\text{nn}}^{\xi}, \quad (1.30)$$

where

$$\xi = -\Psi(0). \quad (1.31)$$

The exponent  $\xi$  is fully determined by the dynamic functions  $M_0(x)$ ,  $M_1(x)$  and  $M_2(x)$  through the Hahn expansion in (1.29). It is independent of  $A_{ij}$ , as well as of other microscopic parameters, such as the specific rate-constants used in (1.1), which are encapsulated within the *coefficients*  $G_n$ , but have no impact on the *powers*  $\Psi(n)$ .

Using approximation (1.24) we substitute  $M_2(x_{\text{nn}})$  in (1.30), to replace the  $\langle M_2(x) \rangle_{\odot}$  term in the denominator of Eq. (1.19), obtaining

$$q \sim \kappa_{\text{nn}}^{-\xi} k^{-1}. \quad (1.32)$$

Next we use these results, specifically (1.18) and (1.32), to obtain the terms of the Jacobian,  $J_{ij}$  and  $J_{ii}$ , and their dependence on  $\kappa_{\text{nn}}$  and  $k$ .

## 1.2 Diagonal terms $D_{ii}$

Using (1.2) and (1.4) we write the diagonal Jacobian terms as

$$D_{ii} = \left. \frac{\partial F_i(\mathbf{x})}{\partial x_i} \right|_{\mathbf{x}=\mathbf{x}^*} = \left( M_0'(x_i) + M_1'(x_i) \sum_{j=1}^N A_{ij} M_2(x_j) \right) \Big|_{\mathbf{x}=\mathbf{x}^*}, \quad (1.33)$$

where  $M_0'(x) = \partial M_0 / \partial x$  and  $M_1'(x) = \partial M_1 / \partial x$ . Next we use (1.10) to express the sum on the r.h.s. obtaining

$$D_{ii} = M_0'(x_i) \Big|_{\mathbf{x}=\mathbf{x}^*} + M_1'(x_i) k_i \langle M_2(x) \rangle_{i,\odot} \Big|_{\mathbf{x}=\mathbf{x}^*}, \quad (1.34)$$

in which we substitute the summation by the neighbor average  $\langle M_2(x) \rangle_{i,\odot}$ . Finally, expressing the fixed-point  $\mathbf{x}^*$  via (1.11) and averaging over all nodes with degree  $k$  as done in (1.13) - (1.19), we arrive at

$$D(k) = M_0'(R^{-1}(q)) + k M_1'(R^{-1}(q)) f(k) \langle M_2(x) \rangle_{\odot}, \quad (1.35)$$

capturing the average diagonal term  $D_{ii}$ , associated with a node  $i \in \mathbf{G}(k)$ .

Next we use (1.8) to write  $M_0(x) = -M_1(x)/R(x)$ , which provides

$$M_0'(x) = -\frac{M_1'(x)}{R(x)} + \frac{M_1(x)R'(x)}{R^2(x)}. \quad (1.36)$$

Substituting (1.36) and (1.19) into (1.35) we arrive at

$$D(k) = -\frac{M_1'(R^{-1}(q))}{q} + \frac{M_1(R^{-1}(q))R'(R^{-1}(q))}{q^2} + \frac{M_1'(R^{-1}(q))}{q}, \quad (1.37)$$

where we used the fact that  $R(R^{-1}(q)) = q$ . Collecting all terms we write

$$D(k) = \frac{1}{q^2}Y(R^{-1}(q)), \quad (1.38)$$

where  $Y(x) = M_1(x)R'(x)$ , similar to  $Z(x)$  above, is a dynamic function fully determined by  $M_0(x)$  and  $M_1(x)$ , independent of  $A_{ij}$ .

To obtain the asymptotic scaling of  $D(k)$  with  $k$  we, once again, use the Hahn expansion to express  $Y(x)$  in the form of a power series around  $q \rightarrow 0$ , *i.e.*  $k \rightarrow \infty$ . Writing

$$Y(R^{-1}(q)) = \sum_{n=0}^{\infty} C_n q^{\Gamma(n)}, \quad (1.39)$$

we obtain the leading power in the expansion of  $D(k)$  as  $D(k) \sim q^{-2+\Gamma(0)}$ , exact up to higher powers in  $q$ , which vanish under  $q \rightarrow 0$ . Using the scaling of Eq. (1.32), this predicts

$$D(k) \sim \kappa_{\text{nn}}^{\xi\mu} k^{\mu}, \quad (1.40)$$

where

$$\mu = 2 - \Gamma(0), \quad (1.41)$$

and  $\xi$  is taken from (1.31).

Equation (1.40), valid in the limit of large  $\kappa_{\text{nn}}$  and  $k$ , captures the typical magnitude of the diagonal terms  $D_{ii}$ , and their dependence on each node  $i$ 's degree  $k_i$ . The scaling exponents  $\mu$  and  $\xi$  are fully determined by  $\Gamma(n)$  in (1.39) and  $\Psi(n)$  in (1.29), namely they are affected by the *powers* of the dynamic functions  $M_0(x)$  and  $M_1(x)$ . At the same time  $\mu$  and  $\xi$  are independent of the *coefficients*  $C_n, G_n$ , hence they are not sensitive to specific parameters, such as rate constants in (1.1). While Eq. (1.40) provides the *scaling* with  $k$ ,  $D(k)$ 's specific magnitude may, generally, depend on the coefficients, however for sufficiently large  $k$ , such dependencies have little impact on the spectrum of  $J_{ij}$ . Finally, the sign of  $D(k)$ , positive or negative, is determined by  $Y(x)$ , which, in turn depends on  $M_0(x)$  and  $M_1(x)$ . Stability can only be ensured in case  $D(k) < 0$ , *i.e.* negative self-feedback, and hence below we write

$$D(k) \sim -C \kappa_{\text{nn}}^{\xi\mu} k^{\mu}, \quad (1.42)$$

where  $C > 0$  (see more detailed discussion in Sec. 1.4).

### 1.3 The off-diagonal terms $W_{ij}$

The off-diagonal Jacobian terms are given by

$$W_{ij} = \left. \frac{\partial F_i(\mathbf{x})}{\partial x_j} \right|_{\mathbf{x}=\mathbf{x}^*} = \left. \frac{\partial}{\partial x_j} \left( M_0(x_i) + M_1(x_i) \sum_{j=1}^N A_{ij} M_2(x_j) \right) \right|_{\mathbf{x}=\mathbf{x}^*}. \quad (1.43)$$

Collecting only the terms that explicitly depend on  $x_j$  we obtain

$$W_{ij} = M_1(x_i) A_{ij} M_2'(x_j) \Big|_{\mathbf{x}=\mathbf{x}^*}, \quad (1.44)$$

which, taking the fixed-point activities from (1.11) provides

$$W_{ij} = M_1(R^{-1}(q_i)) A_{ij} M_2'(R^{-1}(q_j)). \quad (1.45)$$

We seek the average dependence of  $W_{ij}$  on the degrees  $k_i$  and  $k_j$ , hence we consider the group  $\mathbf{G}(k_1, k_2) = \{(i, j) | k_i = k_1; k_j = 2; A_{ij} = 1\}$ , comprising all links ( $A_{ij} = 1$ ) linking nodes with degrees  $k_1, k_2$ . We then average over the relevant Jacobian term as

$$W(k_1, k_2) = \frac{1}{|\mathbf{G}(k_1, k_2)|} \sum_{(i,j) \in \mathbf{G}(k_1, k_2)} W_{ij}, \quad (1.46)$$

allowing us to evaluate the magnitude of an average (non zero) term whose row index is associated with a node of degree  $k_1$ , and whose column index is associated with a node of degree  $k_2$ . Using (1.44) we write

$$W(k_1, k_2) = \frac{1}{|\mathbf{G}(k_1, k_2)|} \sum_{(i,j) \in \mathbf{G}(k_1, k_2)} M_1(x_i) A_{ij} M_2'(x_j) = \langle M_1(x_i) M_2'(x_j) \rangle_{\mathbf{G}(k_1, k_2)}, \quad (1.47)$$

a product average over all node pairs in  $\mathbf{G}(k_1, k_2)$ . In case the two activities  $x_i$  and  $x_j$  are uncorrelated, we can approximate the r.h.s. of (1.47) by a product over the single averages, *i.e.*  $\langle M_1(x_i) \rangle_{\mathbf{G}(k_1, k_2)} \langle M_2'(x_j) \rangle_{\mathbf{G}(k_1, k_2)}$ . Each of these averages can be then evaluated by

$$\langle M_1(x_i) \rangle_{\mathbf{G}(k_1, k_2)} \approx M_1(R^{-1}(q_1)) \quad (1.48)$$

$$\langle M_2'(x_j) \rangle_{\mathbf{G}(k_1, k_2)} \approx M_2'(R^{-1}(q_2)), \quad (1.49)$$

where we use the fact that in  $\mathbf{G}(k_1, k_2)$  the activity  $x_i$  is on average  $R^{-1}(q_1)$ , *i.e.*  $x(k_1)$  (1.13), and the activity  $x_j$  is  $R^{-1}(q_2)$ , namely  $x(k_2)$ . In reality, however, the two activities are, to some extent, correlated by virtue of being nearest neighbors ( $A_{ij} = 1$ ). We therefore follow a similar track as in (1.15) and write (1.47) as

$$W(k_1, k_2) \approx f(k_1, k_2) M_1(R^{-1}(q_1)) M_2'(R^{-1}(q_2)), \quad (1.50)$$

capturing these correlations via the sub-polynomial function  $f(k_1, k_2)$ .

We can now obtain the scaling of  $W(k_1, k_2)$  by examining the behavior of  $M_1(R^{-1}(q_1))$  and  $M_2'(R^{-1}(q_2))$  in the limit of large  $k_1$  and  $k_2$ , or subsequently small  $q_1, q_2$ . We, therefore express these functions via the Hahn expansion as

$$M_1(R^{-1}(q)) = \sum_{n=0}^{\infty} K_n q^{\Pi(n)} \quad (1.51)$$

$$M_2'(R^{-1}(q)) = \sum_{n=0}^{\infty} L_n q^{\Theta(n)}, \quad (1.52)$$

and take only the leading term in the limit  $q \rightarrow 0$ , providing

$$W(k_1, k_2) = f(k_1, k_2) K_0 q_1^{\Pi(0)} L_0 q_2^{\Theta(0)} + \dots \quad (1.53)$$

As we are only interested in the asymptotic scaling with  $k_1, k_2$  we neglect all terms that do not contribute the scaling, namely  $f(k_1, k_2), K_0$  and  $L_0$ . Finally, substituting  $q$  with  $\kappa_{\text{nn}}^{-\xi} k^{-1}$  as per Eq. (1.32), we obtain

$$W(k_1, k_2) \sim \kappa_{\text{nn}}^{\xi(\nu+\rho)} k_1^{\nu} k_2^{\rho} \quad (1.54)$$

where

$$\nu = -\Pi(0), \quad \rho = -\Theta(0), \quad (1.55)$$

and  $\xi$  is taken from (1.31).

#### 1.4 Piecing together the $J_{ij}$ puzzle

We have now obtained the interplay between structure and dynamics, expressed through the magnitude of the diagonal/off-diagonal Jacobian entries, and their dependence on the network's degree distribution via  $k_i, k_j$  and  $\kappa_{\text{nn}}$ . This dependence is given in terms of asymptotic scaling relationships, as captured by the model dependent exponents  $\mu, \nu, \rho, \xi$ . This leaves a degree of freedom, determined by the specific parameters of each model to add an arbitrary coefficient as a pre-factor to the actual  $J_{ij}$  terms. For example, the expression  $D(k) \sim -C \kappa_{\text{nn}}^{\xi \mu} k^{\mu}$  in Eq. (1.40) should be taken to mean

$$D(k) = -C(\kappa_{\text{nn}}, k) \kappa_{\text{nn}}^{\xi \mu} k^{\mu} + \dots \quad (1.56)$$

where  $C(\kappa_{\text{nn}}, k)$  is a sub-polynomial function, which is roughly constant, *i.e.*  $C(\kappa_{\text{nn}}, k) \approx C$ , and  $\dots$  represents *lower* powers of  $\kappa_{\text{nn}}$  and  $k$ , that are negligible in the asymptotic limit. In the context of stability the diagonal terms of  $J_{ij}$  are assumed to be negative, capturing a stabilizing negative feedback, hence the  $-C$  term in (1.56), which is negative if  $C > 0$ .

We can now piece our results together to construct the complete Jacobian as appears in Eq. (1.5), rewriting it as

$$J_{ij} = A_{ij} W_{ij} + \delta_{ij} D_{ii} = -\delta_{ij} C \kappa_{\text{nn}}^{\xi \mu} k_i^{\mu} + A_{ij} \kappa_{\text{nn}}^{\xi(\nu+\rho)} k_i^{\nu} k_j^{\rho}, \quad (1.57)$$

where the first term on the r.h.s. represents the (negative) diagonal entries, and second term captures the off-diagonal entries, which are non-zero only if  $A_{ij} = 1$ ;  $\delta_{ij}$  is the Kronecker delta function. As we are only interested in the sign of the principle eigenvalue, but not in its specific

magnitude, we have the degree of freedom to multiply  $J_{ij}$  by an arbitrary constant. We therefore normalize  $J_{ij}$  by  $\kappa_{\text{nn}}^{-\xi(\nu+\rho)}$ , providing

$$J_{ii} \sim -C\kappa_{\text{nn}}^{\eta}k_i^{\mu} \quad (1.58)$$

$$J_{ij} \sim A_{ij}k_i^{\nu}k_j^{\rho} \quad (1.59)$$

for the diagonal and off-diagonal terms respectively, with  $\eta = \xi(\mu - \nu - \rho)$  - recovering Eqs. (7) and (8) of the main text.

Equations (1.58) and (1.59) describe the asymptotic structure of the diagonal and off-diagonal Jacobian terms, as extracted from the general dynamics of Eq. (1.1). The resulting  $J_{ij}$  is characterized by 6 distinct inputs:  $A_{ij}$ , the network topology, which determines the non-vanishing off-diagonal elements. It also determines the degrees  $k_i, k_j$  and the average neighbor degree  $\kappa_{\text{nn}}$ . The exponents

$$\Omega = (\eta, \mu, \nu, \rho) \quad (1.60)$$

are fully independent of the network topology, extracted from the dynamic functions  $M_0(x), M_1(x)$  and  $M_2(x)$ , *i.e.* the interaction mechanisms driving Eq. (1.1). These exponents are universal in the sense that they do not depend of the specific model *parameters*, but rather on the *model* itself, *e.g.*,  $\mathbb{E}, \mathcal{B}, \mathcal{R}$ , etc. The coefficient  $C$ , in contrast, is non-universal, and its value is determined by the specific rate-constants and time-scales driving Eq. (1.1); here we do not attempt to predict the magnitude of this coefficient. In the limit of sufficiently large  $k_i$  and  $k_j$ , and, where applicable - in the limit of large  $\kappa_{\text{nn}}$ , the specific finite value of  $C$  has negligible impact on the principle eigenvalue of  $J_{ij}$  as we explicitly show in Sec. 3. Hence stability is asymptotically determined by the exponents  $\Omega$ , independent of  $C$ . The meaning is that the *model* can be asymptotically stable or unstable, regardless of its specific *parameters*.

#### 1.4.1 Impact of $P(k)$ and $\kappa_{\text{nn}}$

In this derivation we considered only the *scaling* of  $J_{ij}$  on the degrees  $k_i, k_j$ , and on the nearest neighbor degree  $\kappa_{\text{nn}}$ . We disregarded coefficients, such as  $C_n$  or  $G_n$  in (1.39) and (1.29), or sub-polynomial functions like  $f(k)$  in (1.17). The rationale is that in the limit of large degrees the Jacobian spectrum is mainly impacted by these asymptotic scaling relationships, and has little dependence on finite size coefficients that do not scale with  $k, \kappa_{\text{nn}}$ , and hence also do not grow significantly as a function of system size  $N$ . Indeed, May's paradox is rooted precisely in such scaling, in which the principle eigenvalue grows asymptotically as  $\sim N^c$  (in May's work  $c = 1/2$ ) rendering stability independent of finite coefficients, such as the system's intrinsic time-scales<sup>6</sup>. Therefore, Eqs. (1.58) and (1.59) are especially relevant when  $P(k)$  is fat-tailed, *e.g.*, scale-free, where the hub-degrees and the nearest neighbor degree can potentially scale with  $N$ .

**The role of  $\kappa_{\text{nn}}$ .** While  $k_i$  is a node specific attribute, that captures a specific dependency between the  $i$ th diagonal term and  $i$ 's degree, the pre-factor  $\kappa_{\text{nn}}^{\eta}$  represents a network aggregated parameter, indeed - a *constant*, whose impact is often negligible in the asymptotic limit of large  $k$ . We include it in our analysis, however, because under extreme degree-heterogeneity, we may observe that  $\kappa_{\text{nn}}$  diverges as  $\kappa_{\text{nn}} \sim N^{\beta}$ , and therefore *can* potentially impact the system stability under  $N \rightarrow \infty$ . For example, in a scale-free network where  $P(k) \sim k^{-\gamma}$ , we can use

$\kappa_{\text{nn}} = \langle k^2 \rangle / \langle k \rangle$  in (1.23) to obtain

$$\kappa_{\text{nn}} \sim \begin{cases} N & \gamma < 2 \\ N^{3-\gamma} & 2 \leq \gamma < 3 \\ \log(N) & \gamma \geq 3 \end{cases}, \quad (1.61)$$

which scales with  $N$  as long as  $\gamma < 3$ . There are, however, broad conditions, that arise quite naturally in many real systems, in which the  $\kappa_{\text{nn}}$  term in (1.58) can be neglected, significantly simplifying the stability analysis:

- **Finite  $\kappa_{\text{nn}}$ .** In case  $\gamma \geq 3$ ,  $\kappa_{\text{nn}}$  no longer scales with  $N$ , it behaves as a constant and has no impact in the asymptotic limit. Under these conditions it suffices to write Eq. (1.58) as  $J_{ii} \sim -Ck_i^\mu$ .
- **Bounded activities.** In some models the activities  $x_i$  are bounded. For example, in spreading processes, from epidemics to cascading failures, the activities satisfy  $0 \leq x_i \leq 1$ . Under these conditions the leading power in the power-series expansion of (1.18) is zero, and hence  $x(k \rightarrow \infty) \sim 1$ . The result is that the nearest neighbor activity  $x_{\text{nn}}$ , associated with degree  $\kappa_{\text{nn}}$  is itself bounded, and even if  $\kappa_{\text{nn}} \rightarrow \infty$  *à la* Eq. (1.61), we still have  $x_{\text{nn}} \sim 1$ . Consequently  $M_2(x_{\text{nn}})$  in (1.28) also approaches a constant value, and therefore the leading power in the expansion (1.29) is  $\Psi(0) = 0$ . This provides, based on Eq. (1.31),  $\xi = 0$ , which in turn leads to  $\eta = 0$  in (1.58), again resulting in  $J_{ii} \sim -Ck_i^\mu$ , independent of  $\kappa_{\text{nn}}$ .
- **Saturating  $M_2(x)$ .** Another common feature in many relevant models is that  $M_2(x_j \rightarrow \infty) \rightarrow 1$ . This represents the saturating impact of node  $j$  on its nearest neighbor  $i$ , as frequently observed in regulatory processes or in population dynamics. Once again, we have  $M_2(x_{\text{nn}}) \sim 1$ , providing  $\xi = 0$ , and consequently  $\eta = 0$  in (1.58).

## The ensemble $\mathbb{E}(A_{ij}, \Omega)$ summary

Starting from Eq. (1.1) we use  $M_0(x)$ ,  $M_1(x)$  and  $M_2(x)$  to construct the functions

$$R(x) = -\frac{M_1(x)}{M_0(x)}, \quad Y(x) = M_1(x)R'(x), \quad Z(x) = R(x)M_2(x). \quad (1.62)$$

From these we extract the four relevant power-series expansions

$$\begin{aligned} M_2(Z^{-1}(x)) &= \sum_{n=0}^{\infty} G_n x^{\Psi(n)}, & Y(R^{-1}(x)) &= \sum_{n=0}^{\infty} C_n x^{\Gamma(n)}, \\ M_1(R^{-1}(x)) &= \sum_{n=0}^{\infty} K_n x^{\Pi(n)}, & M_2'(R^{-1}(x)) &= \sum_{n=0}^{\infty} L_n x^{\Theta(n)} \end{aligned} \quad (1.63)$$

whose leading powers determine the dynamic exponents  $\Omega = (\eta, \mu, \nu, \rho)$  as

$$\mu = 2 - \Gamma(0), \quad \nu = -\Pi(0), \quad \rho = -\Theta(0), \quad \eta = -\Psi(0)(\mu - \nu - \rho). \quad (1.64)$$

To construct  $J_{ij} \in \mathbb{E}(A_{ij}, \Omega)$  we first generate the network  $A_{ij}$ , then extract the degrees  $k_i$  of all nodes and the nearest neighbor degree  $\kappa_{\text{nn}}$  from Eq. (1.22). The resulting  $J_{ij}$  satisfies

$$J_{ii} \sim -C \kappa_{\text{nn}}^{\eta} k_i^{\mu} \quad (1.65)$$

$$J_{ij} \sim A_{ij} k_i^{\nu} k_j^{\rho}, \quad (1.66)$$

where the constant  $C > 0$  is arbitrary.

## 2 Analyzing the dynamic models

To demonstrate our formalism we examined several commonly used dynamic models, as listed in Fig. 1g of the main text. Below we extract the exponents  $\Omega$  for each of these models.

### 2.1 Social dynamics

As an example of Social dynamics we used epidemic spreading via the Susceptible-Infected-Susceptible (SIS) model, in which  $x_i(t)$  captures the probability of infection of node  $i$ . Denoting the susceptible state by  $S$  and the infected state by  $I$ , the model includes the following transitions



capturing the processes of recovery at a rate  $f$  and infection at rate  $g$ . This gives rise to the dynamic equation<sup>7</sup>

$$\frac{dx_i}{dt} = -fx_i + \sum_{j=1}^N A_{ij}g(1-x_i)x_j, \quad (2.3)$$

characterized by the dynamic functions  $M_0(x) = -fx$ ,  $M_1(x) = 1 - x$  and  $M_2(x) = gx$ .

To obtain the relevant  $J_{ij}$  ensemble, we seek the exponents  $\Omega = (\eta, \mu, \nu, \rho)$ . We begin by translating the given functions  $M_0(x), M_1(x), M_2(x)$  in to the relevant functions shown in (1.62), providing

$$R(x) = -\frac{M_1(x)}{M_0(x)} = \frac{1-x}{fx} \quad (2.4)$$

$$Y(x) = M_1(x)R'(x) = \frac{x-1}{fx^2} \quad (2.5)$$

$$Z(x) = R(x)M_2(x) = \frac{g}{f} - \frac{g}{f}x. \quad (2.6)$$

Inverting  $R(x)$  and  $Z(x)$ , we write

$$R^{-1}(x) = \frac{1}{fx+1}, \quad (2.7)$$

$$Z^{-1}(x) = 1 - \frac{f}{g}x, \quad (2.8)$$

allowing us to construct the Hahn expansions of (1.63) as

$$M_2(Z^{-1}(x)) = gZ^{-1}(x) = g - fx \quad (2.9)$$

$$Y(R^{-1}(x)) = \frac{R^{-1}(x) - 1}{f \times (R^{-1}(x))^2} = -x - fx^2 \quad (2.10)$$

$$M_1(R^{-1}(x)) = 1 - R^{-1}(x) = \frac{fx}{fx + 1} = fx - f^2x^2 + f^3x^3 - \dots \quad (2.11)$$

$$M_2'(R^{-1}(x)) = g. \quad (2.12)$$

Each of these functions can be expressed as a Hahn power-series, in some cases a finite polynomial, *e.g.*, (2.9) or (2.10), and in others an infinite series, where we only write the leading terms around  $x \rightarrow 0$ . Here, coincidentally, the last function (2.12) is a constant, with the only power being  $x^0$ . We can list the relevant powers in these Hahn expansions as  $\Psi(0) = 0, \Gamma(0) = 1, \Pi(0) = 1$  and  $\Theta(0) = 0$ , which, using (1.64) provides

$$\mu = 2 - \Gamma(0) = 1 \quad (2.13)$$

$$\nu = -\Pi(0) = -1 \quad (2.14)$$

$$\rho = -\Theta(0) = 0 \quad (2.15)$$

$$\eta = -\Psi(0)(\mu - \nu - \rho) = 0. \quad (2.16)$$

## 2.2 Regulatory dynamics

We used the Michaelis-Menten model to capture gene Regulatory dynamics<sup>8</sup>. Here, Eq. (1.1) tracks the level of gene expression  $x_i(t)$ , as regulated via the sub-cellular network  $A_{ij}$ , providing

$$\frac{dx_i}{dt} = -Bx_i^a + \sum_{j=1}^N A_{ij} \frac{x_j^h}{1 + x_j^h}. \quad (2.17)$$

The self-dynamic term  $M_0(x) = -Bx^a$  captures biochemical processes<sup>9</sup>, such as degradation ( $a = 1$ ) or dimerization ( $a = 2$ ). The interaction terms  $M_1(x) = 1, M_2(x) = x^h/1 + x^h$  describe genetic activation, a switch-like dynamics, which ranges from  $M_2(0) = 0$  to  $M_2(x \rightarrow \infty) = 1$  to capture activation of gene  $i$  by gene  $j$ . The Hill coefficient  $h$  governs the rate of saturation of  $M_2(x)$ .

First, we construct the three functions summarized in (1.62):

$$R(x) = -\frac{M_1(x)}{M_0(x)} = \frac{1}{Bx^a} \quad (2.18)$$

$$Y(x) = M_1(x)R'(x) = -\frac{a}{Bx^{a+1}} \quad (2.19)$$

$$Z(x) = R(x)M_2(x) = \frac{x^h}{B(x^a + x^{a+h})}. \quad (2.20)$$

Inverting  $R(x)$ , we write

$$R^{-1}(x) = B^{-\frac{1}{a}} x^{-\frac{1}{a}}, \quad (2.21)$$

allowing us to construct the Hahn expansions (1.63)

$$Y(R^{-1}(x)) = -\frac{a}{B} \left( \frac{1}{Bx} \right)^{-\frac{a+1}{a}} = aB^{\frac{1}{a}} x^{\frac{a+1}{a}} \quad (2.22)$$

$$M_1(R^{-1}(x)) = 1 = x^0 \quad (2.23)$$

$$M_2'(R^{-1}(x)) = \frac{hB^{-\frac{h-1}{a}} x^{-\frac{h-1}{a}}}{\left(1 + B^{-\frac{h}{a}} x^{-\frac{h}{a}}\right)^2} = hB^{\frac{h+1}{a}} x^{\frac{h+1}{a}} - 2hB^{\frac{2h+1}{a}} x^{\frac{2h+1}{a}} + \dots \quad (2.24)$$

In each of these expansions we write the leading terms in the  $x \rightarrow 0$  limit: in (2.22) and (2.23) the expansion features a single term, *i.e.* a pure monomial, and in (2.24) we show the first two terms of the relevant Hahn expansion. To obtain  $\Omega$  we extract only the leading *powers*  $\Gamma(0) = (a+1)/a$ ,  $\Pi(0) = 0$ ,  $\Theta(0) = (h+1)/a$ , ignoring the *coefficients*, *e.g.*,  $aB^{1/a}$  or  $hB^{(h+1)/a}$ . We can now use (1.64) to extract the dynamic exponents as

$$\mu = 2 - \Gamma(0) = \frac{a-1}{a} \quad (2.25)$$

$$\nu = -\Pi(0) = 0 \quad (2.26)$$

$$\rho = -\Theta(0) = -\frac{h+1}{a}. \quad (2.27)$$

To obtain  $\eta$  we must calculate  $M_2(Z^{-1}(x))$ , requiring us to invert the function  $Z(x)$  in (2.20), which becomes analytically prohibitive for general  $a$  and  $h$ . Fortunately, in Regulatory dynamics we can calculate this term directly. We first recall, from Eq. (1.28) that  $M_2(Z^{-1}(q_{\odot})) = M_2(x_{\text{nn}})$ , where  $x_{\text{nn}}$  is the average neighbor activity and  $q_{\odot} \sim 1/\kappa_{\text{nn}}$  is the average neighbor degree. For a general node with degree  $k$  we can use (1.18) together with (2.21) to write

$$x(k) = B^{-\frac{1}{a}} q^{-\frac{1}{a}} \sim k^{\frac{1}{a}}, \quad (2.28)$$

a positive scaling with  $k$ , predicting that  $x(k \rightarrow \infty) \rightarrow \infty$ , namely that a node's activity increases with its degree. Consequently, under a sufficiently large  $\kappa_{\text{nn}}$ , the nearest neighbor activity  $x_{\text{nn}}$  also diverges as  $\kappa_{\text{nn}}^{1/a}$ , or alternatively, as  $q_{\odot}^{-1/a}$ . Hence we write

$$M_2(x_{\text{nn}}) = \frac{x_{\text{nn}}^h}{1 + x_{\text{nn}}^h} \sim \frac{q_{\odot}^{-\frac{h}{a}}}{1 + q_{\odot}^{-\frac{h}{a}}} = \frac{1}{1 + q_{\odot}^{\frac{h}{a}}} = 1 - q_{\odot}^{\frac{h}{a}} + \dots, \quad (2.29)$$

observing directly that the leading power of  $M_2(x_{\text{nn}})$ , and therefore also of  $M_2(Z^{-1}(x))$  is  $\Psi(0) = 0$ . As a result, we obtain, using (1.64) our final exponent

$$\eta = -\Psi(0)(\mu - \nu - \rho) = 0. \quad (2.30)$$

This is, in fact, precisely the case of *Bounded*  $M_2(x)$ , discussed in Sec. 1.4.1, for which we *a priori* predicted  $\eta = 0$ .

## 2.3 Ecological dynamics

We consider mutualistic eco-systems, such as plant-pollinator networks, in which the interacting species exhibit symbiotic relationships. The species populations follow the dynamic equation

$$\frac{dx_i}{dt} = Bx_i(t) \left( 1 - \frac{x_i(t)}{Q} \right) + \sum_{j=1}^N A_{ij}x_j(t)F(x_j(t)). \quad (2.31)$$

The self dynamics

$$M_0(x) = Bx \left( 1 - \frac{x}{Q} \right) \quad (2.32)$$

captures logistic growth: when the population is small, the species reproduce at a rate  $B$ , yet, as  $x_i$  approaches the carrying capacity of the system  $Q$ , growth is hindered by competition over limited resources<sup>10</sup>. The mutualistic inter-species interactions are captured by  $M_1(x) = x$  and  $M_2(x) = F(x)$ , where  $F(x)$  represents the *functional response*, describing the positive impact that species  $j$  has on species  $i$ . This functional response can take one of several forms<sup>11</sup>:

**Type I:** linear impact

$$F(x) = Mx. \quad (2.33)$$

**Type II:** saturating impact

$$F(x) = \frac{Mx}{1 + Mx}. \quad (2.34)$$

**Type III:** a generalization of Type slowromancapii@, where

$$F(x) = \frac{Mx^h}{1 + Mx^h}. \quad (2.35)$$

In our simulations we used Type slowromancapii@ mutualistic interactions, therefore

$$M_2(x) = \frac{Mx}{1 + Mx}. \quad (2.36)$$

For simplicity, we set all coefficients to  $B = Q = M = 1$ .

For  $R(x)$ ,  $Y(x)$  and  $Z(x)$  we have

$$R(x) = -\frac{M_1(x)}{M_0(x)} = \frac{1}{x-1} \quad (2.37)$$

$$Y(x) = M_1(x)R'(x) = -\frac{x}{(x-1)^2} \quad (2.38)$$

$$Z(x) = R(x)M_2(x) = \frac{x}{x^2-1}. \quad (2.39)$$

Inverting  $R(x)$  and  $Z(x)$ , we write

$$R^{-1}(x) = \frac{x+1}{x}, \quad (2.40)$$

$$Z^{-1}(x) = \frac{1}{2x} \left( 1 + \sqrt{1+4x^2} \right), \quad (2.41)$$

where in  $Z^{-1}(x)$  we choose the positive solution, corresponding to the non-zero fixed-point of (2.31). Next, we construct the Hahn expansions of (1.63) as

$$M_2(Z^{-1}(x)) = \frac{Z^{-1}(x)}{1+Z^{-1}(x)} = \frac{1+\sqrt{1+4x^2}}{2x+1+\sqrt{1+4x^2}} = 1-x+\dots \quad (2.42)$$

$$Y(R^{-1}(x)) = -\frac{R^{-1}(x)}{(R^{-1}(x)-1)^2} = x+x^2 \quad (2.43)$$

$$M_1(R^{-1}(x)) = \frac{x+1}{x} = x^{-1}+1 \quad (2.44)$$

$$M_2'(R^{-1}(x)) = \frac{1}{(R^{-1}(x)+1)^2} = \frac{x^2}{4x^2+4x+1} = x^2-4x^3+\dots, \quad (2.45)$$

whose leading powers are  $\Psi(0) = 0, \Gamma(0) = 1, \Pi(0) = -1$  and  $\Theta(0) = 2$ . Consequently, the dynamic exponents in (1.64) are

$$\mu = 2 - \Gamma(0) = 1 \quad (2.46)$$

$$\nu = -\Pi(0) = 1 \quad (2.47)$$

$$\rho = -\Theta(0) = -2 \quad (2.48)$$

$$\eta = \Psi(0)(\mu - \nu - \rho) = 0, \quad (2.49)$$

once again, predicting  $\eta = 0$ , this time thanks both to the *Bounded activities* ( $0 < x_i < Q$ ) and to the *Saturating* nature of the interaction function  $M_2(x)$  (Sec. 1.4.1).

## 2.4 Biochemical dynamics

As a Biochemical model we consider protein-protein interactions (PPI), which are driven by three processes:  $\phi \rightarrow P_i$ , describing the synthesis of the  $i$ th protein  $P_i$  at a rate  $F$ ;  $P_i \rightarrow \phi$ , describing protein degradation at rate  $W$ ;  $P_i + P_j \rightleftharpoons P_i P_j$  describing the binding and unbinding of a pair of interacting proteins at rates  $B$  and  $U$  respectively. The hetero-dimer  $P_i P_j$  undergoes degradation  $P_i P_j \rightarrow \phi$  at rate  $Q$ . The dynamical equations for this system are<sup>9,12</sup>

$$\frac{dx_i}{dt} = F - Wx_i(t) + \sum_{j=1}^N Ux_{ij}(t) - B \sum_{j=1}^N A_{ij}x_i(t)x_j(t) \quad (2.50)$$

$$\frac{dx_{ij}}{dt} = BA_{ij}x_i(t)x_j(t) - (U+Q)x_{ij}(t), \quad (2.51)$$

where  $x_i(t)$  is the concentration of  $P_i$  and  $x_{ij}(t)$  is the concentration of the hetero-dimer  $P_i P_j$ . Under time-scale separation we assume that the hetero-dimer concentration is at steady-state,

setting  $dx_{ij}/dt = 0$  in (2.51). This provides us with

$$\frac{dx_i}{dt} = F - Wx_i(t) - \tilde{B} \sum_{j=1}^N A_{ij}x_i(t)x_j(t), \quad (2.52)$$

where the effective binding rate is  $\tilde{B} = QB/(U + Q)$ . Hence, in the effective equation (2.52) we have  $M_0(x) = F - Wx$ ,  $M_1(x) = -\tilde{B}x$  and  $M_2(x) = x$ , providing the dynamic functions (1.62)

$$R(x) = -\frac{M_1(x)}{M_0(x)} = \frac{\tilde{B}x}{F - Wx} \quad (2.53)$$

$$Y(x) = M_1(x)R'(x) = -\frac{F\tilde{B}^2x}{(F - Wx)^2} \quad (2.54)$$

$$Z(x) = R(x)M_2(x) = \frac{\tilde{B}x^2}{F - Wx}. \quad (2.55)$$

The inverse functions are, therefore

$$R^{-1}(x) = \frac{Fx}{\tilde{B} + Wx} \quad (2.56)$$

$$Z^{-1}(x) = \frac{W}{2\tilde{B}}x \left( -1 + \sqrt{1 + \frac{4\tilde{B}F}{W^2x}} \right), \quad (2.57)$$

where in  $Z^{-1}(x)$  we choose the positive solution, corresponding to the positive fixed-point of (2.52). We can now compose the functions in (1.63), obtaining

$$M_2(Z^{-1}(x)) = Z^{-1}(x) = \sqrt{\frac{F}{\tilde{B}}x^{\frac{1}{2}} + \frac{W^2}{8\tilde{B}^2F^{\frac{1}{2}}}x^{\frac{3}{2}} + \dots} \quad (2.58)$$

$$Y(R^{-1}(x)) = -\frac{F\tilde{B}^2R^{-1}(x)}{(F - WR^{-1}(x))^2} = F\tilde{B}^2x + F\tilde{B}Wx^2 \quad (2.59)$$

$$M_1(R^{-1}(x)) = -\frac{\tilde{B}Fx}{\tilde{B} + Wx} = -Fx + \frac{FW}{\tilde{B}}x^2 + \dots \quad (2.60)$$

$$M_2'(R^{-1}(x)) = 1, \quad (2.61)$$

allowing us to extract the leading powers as  $\Psi(0) = 1/2$ ,  $\Gamma(0) = 1$ ,  $\Pi(0) = 1$  and  $\Theta(0) = 0$ . These powers provide the dynamic exponents via (1.64), providing, for Biochemical

$$\mu = 2 - \Gamma(0) = 1 \quad (2.62)$$

$$\nu = -\Pi(0) = -1 \quad (2.63)$$

$$\rho = -\Theta(0) = 0 \quad (2.64)$$

$$\eta = \Psi(0)(\mu - \nu - \rho) = \frac{1}{2}. \quad (2.65)$$

### 3 Principle eigenvalue of $J_{ij} \in \mathbb{E}(A_{ij}, \Omega)$

The stability of Eq. (1.1) can be characterized by the principal eigenvalue  $\lambda$  of  $J_{ij}$  in (1.65) - (1.66). As the entries depend on  $k_i$  and  $k_j$ , the value of  $\lambda$  is driven by the limit of large  $k$  - specifically, in a degree-heterogeneous network, it is determined by the nearest neighbor degree  $\kappa_{\text{nn}}$ , which can potentially diverge with the system size  $N$  as

$$\kappa_{\text{nn}} \sim N^\beta. \quad (3.1)$$

As opposed to the *dynamic* exponents  $\Omega$ , the exponent  $\beta$  is a *topological* exponent, determined by the network's degree distribution  $P(k)$ . In a scale-free network, for example  $\beta$  is extracted from (1.61).

To approximate this hub-periphery structure, we use a *star* network, in which a single hub is linked to

$$k = \kappa_{\text{nn}} \sim N^\beta \quad (3.2)$$

peripheral nodes. This captures the environment of a typical hub in, *e.g.*, a scale-free network. Indeed, the hubs in a scale-free network can be viewed as a collection of weakly coupled *stars*, that are only sparsely linked to each other<sup>13</sup>. Under these conditions we have the  $(k+1) \times (k+1)$  network

$$A_{ij} = \begin{bmatrix} 0 & 1 & 1 & \dots & 1 \\ 1 & 0 & 0 & \dots & 0 \\ \vdots & & \ddots & & \vdots \\ 1 & 0 & 0 & \dots & 0 \end{bmatrix}, \quad (3.3)$$

which using (1.65) and (1.66), provides the corresponding Jacobian as

$$J_{ij} = -C\tilde{\kappa}_{\text{nn}}^\eta \begin{bmatrix} k^\mu & 0 & \dots & 0 \\ 0 & 1 & \dots & 0 \\ \vdots & & \ddots & \vdots \\ 0 & 0 & \dots & 1 \end{bmatrix} + \begin{bmatrix} 0 & k^\nu & \dots & k^\nu \\ k^\rho & 0 & \dots & 0 \\ \vdots & & \ddots & \vdots \\ k^\rho & 0 & \dots & 0 \end{bmatrix}, \quad (3.4)$$

where  $C > 0$ . In (3.4) we used  $\tilde{\kappa}_{\text{nn}}$  to express the nearest neighbor degree in our star construction, which is potentially distinct from  $\kappa_{\text{nn}}$  of the originally approximated scale-free network. Lacking an *a priori* estimate for this parameter we express it as

$$\tilde{\kappa}_{\text{nn}} \sim N^\alpha, \quad (3.5)$$

leaving us a degree of freedom to later tune  $\alpha$  such that the prediction from our star construction best captures the observed results from a real scale-free network. Hence,  $\beta$ , characterizing the star-hub ( $k$ ) is extracted from  $A_{ij}$  via (3.1) and  $\alpha$  is a tunable parameter, which we select for the star-model to best fit the complete scale-free network results.

We emphasize that the star approximation in (3.3) by no means captures the complete behavior of a real scale-free network, as indeed it represents but a crude representation of an isolated hub environment. However, our goal here is to examine stability vs. instability - a feature that only depends on the *sign* of the principal eigenvalue, not on its specific value, and is, therefore, insensitive to the detailed structure of  $A_{ij}$ . As we show in Fig. 3 of the main text the star approximation, while highly stylized, is, indeed, sufficient to capture this  $J_{ij}$  characteristic.

To obtain the principal eigenvalue we solve the linear equation

$$J\mathbf{v} = \lambda\mathbf{v}. \quad (3.6)$$

Using the symmetry of (3.4), we seek a solution of the form  $\mathbf{v} = (a, b, b, \dots, b)^\top$ , allowing us to reduce (3.6) into

$$-C\tilde{\kappa}_{\text{nn}}^\eta k^\mu a + k k^\nu b = \lambda a \quad (3.7)$$

$$k^\rho a - C\tilde{\kappa}_{\text{nn}}^\eta b = \lambda b. \quad (3.8)$$

Note that in  $\mathbf{v}$  the specific values of  $a, b$  have no significance, only the ratio  $a/b$ , as we are only interested in the *direction* of the eigenvector, not its magnitude. We therefore arbitrarily set  $a = 1$ , allowing us to solve (3.7) - (3.8) and obtain

$$\lambda = \frac{1}{2} \left( -C\tilde{\kappa}_{\text{nn}}^\eta (k^\mu + 1) + \sqrt{C^2 \tilde{\kappa}_{\text{nn}}^{2\eta} (k^\mu + 1)^2 - 4C^2 \tilde{\kappa}_{\text{nn}}^{2\eta} k^\mu + 4k^{1+\nu+\rho}} \right), \quad (3.9)$$

where we selected only the positive solution, as we seek the largest eigenvalue. Seeking the limit

$$\lim_{N \rightarrow \infty} (\lambda), \quad (3.10)$$

we use (3.2) and (3.5) to rewrite (3.9) as

$$\lambda \sim \frac{1}{2} \left( -CN^{\alpha\eta} (N^{\beta\mu} + 1) + \sqrt{C^2 N^{2\alpha\eta} (N^{\beta\mu} + 1)^2 + 4 \left[ -C^2 N^{2\alpha\eta + \beta\mu} + N^{\beta(1+\nu+\rho)} \right]} \right), \quad (3.11)$$

in which we replace  $\tilde{\kappa}_{\text{nn}}$  and  $k$  by  $N^\alpha$  and  $N^\beta$ , respectively. In (3.11) we ignore the pre-factors of the  $N$ -scaling, focusing only on the powers  $(\alpha, \beta)$ , hence substituting the equality sign  $=$  with the asymptotic scaling operator  $\sim$ .

**The case where  $\mu > 0$ .** First we analyze  $\lambda$  under  $\mu > 0$ . Here, we write  $N^{\beta\mu} \gg 1$ , simplifying (3.11) in the limit  $N \rightarrow \infty$  into

$$\lambda \sim \frac{1}{2} \left( -CN^{\alpha\eta + \beta\mu} + \sqrt{C^2 N^{2(\alpha\eta + \beta\mu)} + 4 \left[ -C^2 N^{2\alpha\eta + \beta\mu} + N^{\beta(1+\nu+\rho)} \right]} \right). \quad (3.12)$$

Extracting the common terms out of the product we rewrite (3.12) as

$$\lambda \sim \frac{1}{2}CN^{\alpha\eta+\beta\mu} \left( -1 + \sqrt{1 + 4 \left( -N^{-\beta\mu} + \frac{1}{C^2}N^\sigma \right)} \right), \quad (3.13)$$

where

$$\sigma = \beta \left( 1 + \nu + \rho - 2\mu - 2\frac{\alpha}{\beta}\eta \right). \quad (3.14)$$

Note that  $N^{-\beta\mu} \leq 1$  in (3.13), as  $\mu > 0$ . Therefore, in case  $\sigma \geq 0$ , the  $N^\sigma$  term dominates the r.h.s. of the equation, providing, under  $N \rightarrow \infty$ ,

$$\lambda \sim \frac{C}{\sqrt{C^2}} N^{\frac{1}{2}\sigma + \alpha\eta + \beta\mu}, \quad (3.15)$$

which, since  $C > 0$  is guaranteed to be positive, *i.e.* the system is *unstable*.

Next we consider the case  $\sigma < 0$ . Under these conditions  $N^\sigma \ll 1$ , allowing us to expand the square-root in (3.13) to first order, providing

$$\lambda \sim \frac{1}{2}CN^{\alpha\eta+\beta\mu} \left( -1 + 1 + 2 \left( -N^{-\beta\mu} + \frac{1}{C^2}N^\sigma \right) \right) = -CN^{\alpha\eta} + \frac{1}{C}N^{\sigma+\alpha\eta+\beta\mu}. \quad (3.16)$$

We can rewrite this in the form of Eq. (11) of the main text, obtaining

$$\lambda \sim N^Q \left( 1 - \frac{C}{N^S} \right), \quad (3.17)$$

where

$$Q = \sigma + \alpha\eta + \beta\mu \quad (3.18)$$

$$S = \sigma + \beta\mu. \quad (3.19)$$

As  $N^Q$  is guaranteed to be positive, the sign of  $\lambda$  depends on  $S$ : in case  $S > 0$  the negative term in (3.17) satisfies  $CN^{-S} \ll 1$ , and hence we have  $\lambda \sim N^Q > 0$ , an unstable dynamics. If however  $S < 0$ , we have  $-CN^{-S} \rightarrow -\infty$ , predicting  $\lambda < 0$ , regardless of  $C$ , an asymptotically stable system. Consequently the system is stable as long as  $S < 0$ , which using (3.19), and taking  $\sigma$  from (3.14), predicts the stability condition

$$\beta \left( 1 + \nu + \rho - \mu - 2\frac{\alpha}{\beta}\eta \right) < 0. \quad (3.20)$$

This condition reduces stability into a small set of *relevant* parameters:  $\beta$ , characterizing the network topology  $A_{ij}$ , and  $\Omega = (\eta, \mu, \nu, \rho)$ , associated with the dynamics  $M_0(x), M_1(x), M_2(x)$ . The non-universal parameter  $C$  becomes irrelevant in the limit of sufficiently large  $N$ . Finally,  $\alpha$  can be selected to tune the star approximation optimally to the case of a real scale-free  $A_{ij}$ , as we do below. Note that condition (3.20) can also be expressed as  $\sigma + \beta\mu < 0$ . This implies that if  $\sigma > \beta\mu$  the system is unstable. This instability condition already contains the previously obtained condition of  $\sigma > 0$ , that led to Eq. (3.15). Therefore, Eq. (3.20) is sufficient

to characterize the system's stability.

Finally, the case  $S = 0$  in (3.17) represents sensitive stability, in which  $\lambda$ 's value is not asymptotically defined, and rather it depends on the coefficient  $C$ . In this class, stability is no longer a characteristic of the dynamic *model*, but rather of its specific rate constants, as encapsulated within  $C$ . A trivial example is when  $\beta = 0$ , *i.e.* a non fat-tailed  $P(k)$ , for example - Erdős-Rényi. Indeed, as we discuss in the main text, in such networks, stability can be tuned by the model parameters, lacking a defined asymptotic behavior.

**The case where  $\mu \leq 0$ .** Here, we have  $N^{\beta\mu} \leq 1$ , and hence Eq. (3.11) can be approximated by

$$\lambda \sim \frac{1}{2} \left( -CN^{\alpha\eta} + \sqrt{C^2 N^{2\alpha\eta} + 4[-C^2 N^{2\alpha\eta+\beta\mu} + N^{\beta(1+\nu+\rho)}]} \right), \quad (3.21)$$

leading to

$$\lambda \sim \frac{1}{2} CN^{\alpha\eta} \left( -1 + \sqrt{1 + 4 \left( -N^{\beta\mu} + \frac{1}{C^2} N^\omega \right)} \right), \quad (3.22)$$

where

$$\omega = \beta \left( 1 + \nu + \rho - 2 \frac{\alpha}{\beta} \eta \right). \quad (3.23)$$

Once again, we have  $N^{\beta\mu} \leq 1$ , this time since  $\mu < 0$ . Therefore, as before, if  $\omega > 0$ ,  $\lambda$  becomes dominated by the  $N^\omega$  term, following

$$\lambda \sim \frac{C}{\sqrt{C^2}} N^{\frac{1}{2}\omega + \alpha\eta}, \quad (3.24)$$

which is always positive, *i.e.* *unstable*. If, however,  $\omega < 0$ , we use a linear approximation to write

$$\lambda \sim \frac{1}{2} CN^{\alpha\eta} \left( -1 + 1 + 2 \left( -N^{\beta\mu} + \frac{1}{C^2} N^\omega \right) \right) = -CN^{\alpha\eta+\beta\mu} + \frac{1}{C} N^{\omega+\alpha\eta}, \quad (3.25)$$

once again - a competition between a positive vs. a negative term. Collecting the powers we, again, rewrite (3.25) in the form

$$\lambda \sim N^Q \left( 1 - \frac{C}{N^S} \right), \quad (3.26)$$

where this time

$$Q = \omega + \alpha\eta \quad (3.27)$$

$$S = \omega - \beta\mu. \quad (3.28)$$

Stability is ensured if, for  $N \rightarrow \infty$ , the negative term dominates, namely if  $S < 0$ . Using (3.23) to express  $\omega$  this provides

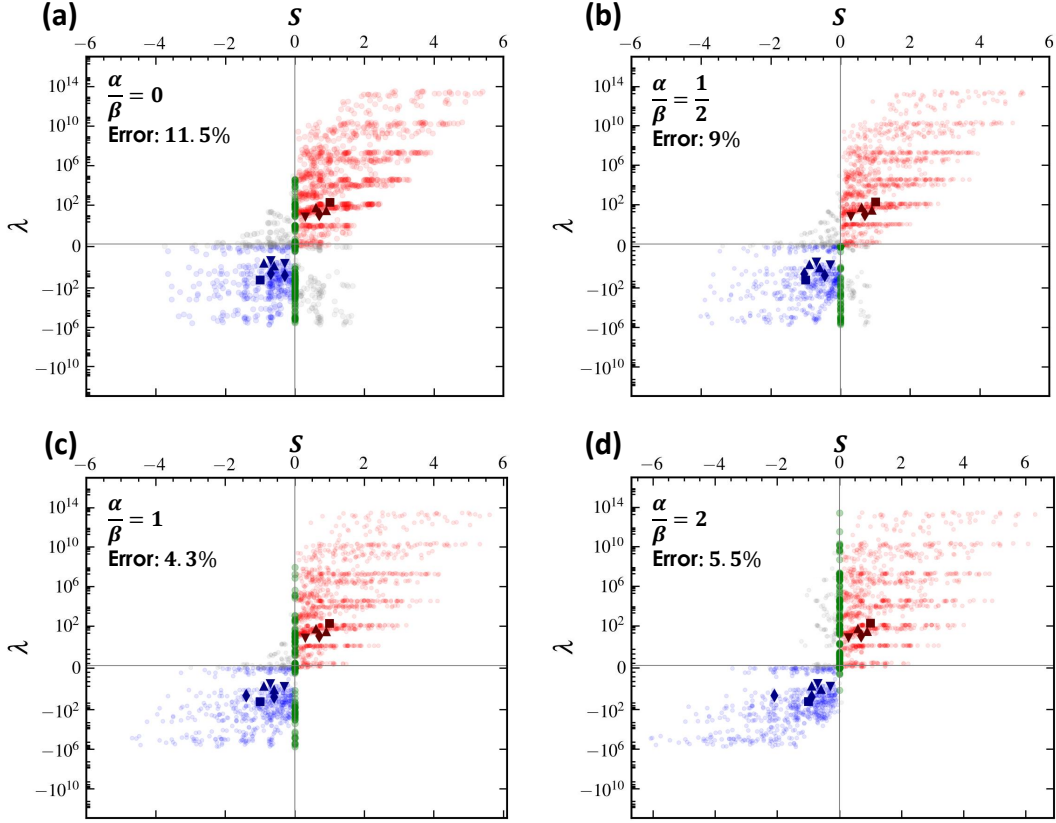


Figure 4: **Tuning the parameter  $\alpha$ .** In Eqs. (3.20) and (3.29) we have the degree of freedom to set  $\alpha/\beta$  for the star approximation to best predict the stability of complete scale-free networks. We used our set of 2,077  $J$  matrices (Fig. 3a of main text) to predict stability using different values of  $\alpha/\beta$ . Quantifying the Error by the fraction of mis-classified  $J$  matrices (grey dots), we find that setting  $\alpha/\beta = 1$  provides the optimal fit, securing a  $\sim 96\%$  correct classification (Error= 4.3%).

$$\beta \left( 1 + \nu + \rho - \mu - 2 \frac{\alpha}{\beta} \eta \right) < 0, \quad (3.29)$$

recovering precisely the condition in (3.20).

**Tuning  $\alpha$ .** The parameter  $\alpha$  represents a degree of freedom, rooted in the fact that the star approximation captures an inaccurate depiction of a real scale-free network. This approximation can be optimized if we select  $\alpha$  such that the star best captures the complete scale-free network environment. We find that setting

$$\alpha = \frac{\beta}{2} \quad (3.30)$$

provides the optimal approximation, accurately predicting stability 96% of the time (Fig. 1). This completes the stability analysis, providing the classifier parameter as

$$S = \beta (1 + \nu + \rho - \mu - \eta), \quad (3.31)$$

as appears in Eq. (10) of the main text.

### 3.1 The role of topology vs. dynamics

The stability condition (3.31) is driven by five distinct exponents. The first four exponents  $\Omega = (\eta, \mu, \nu, \rho)$  are determined by the dynamic model - Social, Regulatory, Ecological etc. - intrinsic to the system's inherent interaction mechanisms. These exponents are independent of the topology  $A_{ij}$  or of microscopic model parameters, encapsulated within  $C$ , and are therefore *hardwired* into the system's dynamic behavior. For example, our formalism predicts that the SIS model (Social) has  $\Omega = (0, 1, -1, 0)$  (Sec. 2.1). This prediction is characteristic to the SIS model, namely it is an intrinsic feature of the SIS interaction mechanisms of infection and recovery. It is, therefore, insensitive to the specific rates of the model - hence  $\Omega$  remains unchanged if, *e.g.*, a disease has a high or low infection rates, or if it is transmitted via physical contact or aerosols. These will impact the constant  $C$  in (1.65), but will have no impact on the universal scaling. Similarly,  $\Omega$  is unaffected by  $A_{ij}$ . Therefore, regardless of whether the disease spreads along the standard social network (Flu) or via sexual transmission (AIDS), as long as the *mechanism* is SIS (or any other mechanism for that matter)  $\Omega$  remains the same.

The remaining exponent in (3.31),  $\beta$ , on the other hand, is independent of the dynamics, and determined solely by  $A_{ij}$ , specifically by its degree distribution  $P(k)$ , capturing the divergence of  $\kappa_{\text{nn}}$  in the limit of large  $N$ . For example, under a scale-free topology, where  $P(k) \sim k^{-\gamma}$ , we have  $\kappa_{\text{nn}}$  following Eq. (1.61), predicting

$$\beta = \begin{cases} 1 & \gamma < 2 \\ 3 - \gamma & 2 \leq \gamma < 3 \\ 0 & \gamma \geq 3 \end{cases} . \quad (3.32)$$

Therefore under  $\gamma \geq 3$ , we have  $\beta = 0$  and stability becomes sensitive to parameters ( $C$ ). On the other hand, under a scale-free topology ( $\gamma < 3$ ) we observe the asymptotic stability/instability driven by  $S \neq 0$ .

## 4 Methods and data analysis

### 4.1 Numerical integration

To numerically test our predictions we constructed Eq. (1.1) for each of the systems in Sec. 2, using the appropriate  $A_{ij}$  (Scale-free, Erdős-Rényi, empirical, etc.). We then used a fourth-order Runge-Kutta stepper (Matlab's ode45) to numerically solve the resulting equations. Starting from an arbitrary initial condition  $x_i(t=0)$ ,  $i = 1, \dots, N$  we allowed the system to reach steady-state by waiting for  $\dot{x}_i \rightarrow 0$ . To numerically realize this limit we implemented the termination condition

$$\max_{i=1}^N \left| \frac{x_i(t_n) - x_i(t_{n-1})}{x_i(t_n) \Delta t_n} \right| < \varepsilon, \quad (4.1)$$

where  $t_n$  is the time stamp of the  $n$ th Runge-Kutta step and  $\Delta t_n = t_n - t_{n-1}$ . As the system approaches a steady-state, the activities  $x_i(t_n)$  become almost independent of time, and the numerical derivative  $\dot{x}_i = x_i(t_n) - x_i(t_{n-1})/\Delta t_n$  becomes small compared to  $x_i(t_n)$ . The condition (4.1) guarantees that the maximum of  $\dot{x}_i/x_i$  over all activities  $x_i(t_n)$  is smaller than the pre-defined termination variable  $\varepsilon$ . In our simulations, across the different dynamics we tested, we set  $\varepsilon \leq 10^{-12}$ , a rather strict condition, to ensure that our system is sufficiently close to the *true* steady-state.

## 4.2 Numerically estimating $J_{ij}$

Once the steady state  $\mathbf{x} = (x_1, \dots, x_N)^\top$  is reached we construct the *numerical* Jacobian by substituting the numerically obtained states  $x_i$  into (1.33) and (1.44). This represents the system's actual stability matrix, incorporating its specific dynamics on the relevant network  $A_{ij}$ . For example, consider our Social model in Eq. (2.3), where  $M_0(x) = -fx$ ,  $M_1(x) = 1 - x$  and  $M_2(x) = gx$ , and hence  $M'_0(x) = -f$ ,  $M'_1 = -1$  and  $M'_2 = g$ . Once we obtain  $\mathbf{x}$  we introduce all numerically calculated  $x_i$  into  $D_{ii}$  and  $Q_{ij}$ , which for Social take the form

$$D_{ii} = -f + - \sum_{j=1}^N A_{ij} g x_j \quad (4.2)$$

and

$$Q_{ij} = A_{ij}(1 - x_i)g. \quad (4.3)$$

In Fig. 2 of the main text we compare the scaling of these numerically estimated  $D_{ii}$  and  $Q_{ij}$  vs. the theoretically predicted ensemble  $\mathbb{E}(A_{ij}, \Omega)$ , shown in (1.65) and (1.66).

## 4.3 Logarithmic binning

Our main theoretical prediction focuses on scaling relationships, such as  $D(k) \sim k^\mu$ , which we observe by their linear slope in a log-log plot. To construct such plots we employed logarithmic binning<sup>14</sup>. First we divide all nodes into  $W$  bins

$$\mathbb{B}(w) = \{i = 1, \dots, N \mid c^{w-1} < k_i \leq c^w\}, \quad (4.4)$$

where  $w = 1, \dots, W$  and  $c$  is a constant. In (4.4) the  $w$ th bin includes all nodes  $i$  whose degrees  $k_i$  are between  $c^{w-1}$  and  $c^w$ . The parameter  $c$  is selected such that the unity of all bins  $\cup_{w=1}^W \mathbb{B}(w)$  includes all nodes, hence we set  $c^W = \max_{i=1}^N k_i$ . We then plot the average degree of the nodes in each bin

$$k_w = \langle k_i \rangle_{i \in \mathbb{B}(w)} = \frac{1}{|\mathbb{B}(w)|} \sum_{i \in \mathbb{B}(w)} k_i \quad (4.5)$$

versus the average  $D_{(k)}$  term of nodes in that bin

$$D(k_w) = \langle D_{ii} \rangle_{i \in \mathbb{B}(w)} = \frac{1}{|\mathbb{B}(w)|} \sum_{i \in \mathbb{B}(w)} D_{ii}. \quad (4.6)$$

In a similar fashion we plot  $Q_{ij} \sim k_i^\nu k_j^\rho$ , this time applying the binning on  $k_i^\nu k_j^\rho$ , instead of  $k_i$ . Therefore, the bins are defined as

$$\mathbb{B}(w) = \{(i, j) | A_{ij} = 1, c^{w-1} < k_i^\nu k_j^\rho \leq c^w\}, \quad (4.7)$$

such that in each bin we include all node pairs whose product  $k_i^\nu k_j^\rho$  is within a given range. As above, we then plot the average  $Q_{ij}$  in each bin, providing the real Jacobian terms

$$J_w^{\text{Real}} = \langle Q_{ij} \rangle_{(i,j) \in \mathbb{B}(w)} = \frac{1}{|\mathbb{B}(w)|} \sum_{(i,j) \in \mathbb{B}(w)} Q_{ij} \quad (4.8)$$

vs. the average value of  $k_i^\nu k_j^\rho$  in that bin

$$J_w^{\text{Th}} = \langle Q_{ij} \rangle_{(i,j) \in \mathbb{B}(w)} = \frac{1}{|\mathbb{B}(w)|} \sum_{(i,j) \in \mathbb{B}(w)} Q_{ij}. \quad (4.9)$$

#### 4.4 Model and empirical networks

To test our predictions we used model and real networks, as summarized below:

**ER.** An Erdős-Rényi random network with  $N = 6,000$  nodes and an average degree of  $\langle k \rangle = 6$ .

**SF1,2,3.** A set of binary scale-free networks, constructed via the configuration model<sup>2</sup>, with  $N = 6,000$  nodes,  $\langle k \rangle = 6$  and degree distribution following  $P(k) \sim k^{-\gamma}$  with  $\gamma = 2, 2.5$  and  $3$ , respectively.

**UCIonline** (Social). An instant messaging network from the University of California Irvine<sup>16</sup>, capturing 61,040 transactions between 1,893 users during a  $T = 218$  day period. Connecting all individuals who exchanged messages throughout the period, we obtain a network of 1,893 nodes with 27,670 links, exhibiting a fat-tailed degree distribution.

**Email Epoch** (Social). This dataset monitors  $\sim 3 \times 10^5$  emails exchanged between 3,185 individuals over the course of  $\sim 6$  months<sup>17</sup>, giving rise to a scale-free social network with 31,885 binary links.

**PPI1** (Regulatory, Biochemical). The yeast scale-free protein-protein interaction network, consisting of 1,647 nodes (proteins) and 5,036 undirected links, representing chemical interactions between proteins<sup>18</sup>.

**PPI2** (Regulatory, Biochemical). The human protein-protein interaction network, a scale-free network, consisting of  $N = 2,035$  nodes (protein) and  $L = 13,806$  protein-protein interaction links<sup>19</sup>.

**ECO1,2** (Ecological). To construct the mutualistic ecological networks we collected data on symbiotic interactions of plants and pollinators in Carlinville Illinois from<sup>22</sup>. The resulting  $456 \times 1,429$  network  $M_{ik}$  is a bipartite graph linking the 456 plants with their 1,429 pollinators. When a pair of plants is visited by the same pollinator they mutually benefit each other indirectly, by increasing the pollinator populations. Similarly pollinators sharing the same plants also posses

an indirect mutualistic interaction. Hence we can collapse  $M_{ik}$  to construct two mutualistic networks: The  $1,429 \times 1,429$  pollinator network ECO1 and the  $456 \times 456$  plant network ECO2. The resulting networks are

$$B_{kl} = \sum_{i=1}^{456} \frac{M_{ik}M_{il}}{\sum_{s=1}^n M_{is}}, \quad (4.10)$$

for the pollinator network (ECO1), and

$$A_{ij} = \sum_{k=1}^{1,429} \frac{M_{ik}M_{jk}}{\sum_{s=1}^n M_{sk}}, \quad (4.11)$$

for the plant network (ECO2). In both networks the numerator equals to the number of mutual plants ( $B_{kl}$ ) or pollinators ( $A_{ij}$ ). For each mutual plant  $i$  (pollinator  $k$ ) we divide by the overall number of plants (pollinators) that share  $i$  ( $k$ ). Hence, the weight of the mutualistic interaction in, *e.g.*,  $A_{ij}$  is determined by the density of mutual symbiotic relationships between all plants, where: (i) the more mutual pollinators  $k$  that plants  $i$  and  $j$  share the stronger the mutualistic interaction between them; (ii) on the other hand the more plants pollinated by  $k$  the smaller is its contribution to each plant. A similar logic applies also for the pollinator network  $B_{ij}$ . This process potentially allows us to have isolated components, *e.g.*, single disconnected nodes. The state of these isolated nodes is decoupled from the state of the rest of the network, and hence in our analysis we only focused on the giant connected component of  $A_{ij}$  and  $B_{ij}$ , comprising all 456 plants, rendering  $A_{ij}$  to be a fully connected component, but only 1,044 pollinators, eliminating 385 isolated pollinators in  $B_{ij}$ .

## References

- [1] B. Barzel and A.-L. Barabási. Universality in network dynamics. *Nature Physics*, 9:673 – 681, 2013.
- [2] M.E.J. Newman. *Networks - an introduction*. Oxford University Press, New York, 2010.
- [3] J. Gao, B. Barzel and A.-L. Barabási. Universal resilience patterns in complex networks. *Nature*, 530:307–312, 2016.
- [4] G. Caldarelli. *Scale-free networks: complex webs in nature and technology*. Oxford University Press, New York, 2007.
- [5] L. Schmetterer and K. Sigmund (Eds.). *Hans Hahn Gesammelte Abhandlungen Band 1/Hans Hahn Collected Works Volume 1*. Springer, Vienna, Austria, 1995.
- [6] R.M. May. Will a large complex system be stable? *Nature*, 238:413 – 414, 1972.
- [7] P.S. Dodds and D.J. Watts. A generalized model of social and biological contagion. *Journal of Theoretical Biology*, 232:587–604, 2005.
- [8] G. Karlebach and R. Shamir. Modelling and analysis of gene regulatory networks. *Nature Reviews*, 9:770–780, 2008.
- [9] B. Barzel and O. Biham. Binomial moment equations for stochastic reaction systems. *Phys. Rev. Lett.*, 106:150602–5, 2011.
- [10] R.M. May. Simple mathematical models with very complicated dynamics. *Nature*, 261: 459–467, 1976.
- [11] C.S. Holling. Some characteristics of simple types of predation and parasitism. *The Canadian Entomologist*, 91:385–398, 1970.
- [12] E.O. Voit. *Computational Analysis of Biochemical Systems*. Cambridge University Press, New York, NY, 2000.
- [13] H.I. Schreier, Y. Soen and N. Brenner. Exploratory adaptation in large random networks. *Nature Communications*, 8:14826, 2017.
- [14] S. Milojević. Power-law distributions in information science: making the case for logarithmic binning. *Journal of the American Society for Information Science and Technology*, 61:2417–2425, 2010.
- [15] A.-L. Barabási and R. Albert. Emergence of scaling in random networks. *Science*, 286: 509–512, 1999.
- [16] T. Opsahl and P. Panzarasa. Clustering in weighted networks. *Social Networks*, 31:155–163, 2009.
- [17] J.-P. Eckmann, E. Moses and D. Sergi. Entropy of dialogues creates coherent structures in e-mail traffic. *Proc. Natl. Acad. Sci. USA*, 101:14333–7, 2004.
- [18] H. Yu *et al.* High-quality binary protein interaction map of the yeast interactome network. *Science*, 322:104–110, 2008.

- [19] J.F. Rual *et al.* Towards a proteome-scale map of the human protein-protein interaction network. *Nature*, 437:1173–1178, 2005.
- [20] K. Ikehara and A. Clauset. Characterizing the structural diversity of complex networks across domains. *arXiv:1710.11304v1*, 333:1–23, 2017.
- [21] E. Bullmore and O. Sporns. Complex brain networks: graph theoretical analysis of structural and functional systems. *Nature Rev. Neuroscience*, 10:3, 2009.
- [22] Interaction web database. <http://www.nceas.ucsb.edu/interactionweb/resources>.